Spectral characteristics of coralline algae: a multi-instrumental approach, with emphasis on underwater hyperspectral imaging

AKSEL ALSTAD MOGSTAD[1, *], GEIR JOHNSEN[1, 2]

[1]*Centre for Autonomous Marine Operations and Systems, Department of Biology, Norwegian University of Science and Technology (NTNU), Trondheim Biological Station, NO-7491 Trondheim, Norway*
[2]*University Centre in Svalbard (UNIS), P.O. Box 156, NO-9171 Longyearbyen, Norway*
Corresponding author: aksel.a.mogstad@ntnu.no

Coralline algae constitute a cosmopolitan group of calcifying rhodophytes (red algae) that display characteristic optical fingerprints due to light absorption by specific light-harvesting pigments. The spectrally conspicuous nature of coralline algae makes them potential candidates for optical remote sensing surveys, and recently, a novel optical remote sensing technique has entered the scene of marine research: underwater hyperspectral imaging (UHI). The aim of the study was to characterize the spectral properties of different coralline algal species, and to assess the potential of UHI as a coralline algal identification and mapping tool. Four species of coralline algae were investigated: *Corallina officinalis*, *Lithothamnion glaciale*, *Phymatolithon lenormandii*, and *Phymatolithon tenue*. Important coralline algal pigments were identified using spectrophotometry and high-performance liquid chromatography (HPLC). Reflectance spectra of all species were obtained using both a spectrometer and UHI. Multivariate statistical analyses were performed on the reflectance data to identify spectral differences between species and instruments. In addition, supervised classification of coralline algae in UHI transects recorded both *in vivo* and *in situ* was carried out. R-phycoerythrin and chlorophyll a were found to be the most dominant coralline algal pigments. The analyzed species of coralline algae displayed highly similar reflectance spectra, and dips in reflectance corresponding to the absorbance peaks of R-phycoerythrin and chlorophyll a were identified in all spectra. Wavelengths corresponding to R-phycoerythrin light absorbance were the greatest contributors to interspecific spectral differences, but the investigated coralline algal species could not be spectrally distinguished with great accuracy. Optical signatures recorded using different instruments were comparable, but inter-instrumental spectral differences were found to be greater than interspecific differences. Supervised UHI classification was unable to accurately map different coralline algal species due to the similarity of the optical fingerprints, but as a group, coralline algae could easily be identified. In the future, large-scale UHI surveys of coralline algal habitats should be carried out using platforms such as remotely operated vehicles (ROVs) and autonomous underwater vehicles (AUVs) to enhance our understanding of this widespread and ecologically important organism group.

1. INTRODUCTION

A. Coralline algae

Coralline algae are multicellular rhodophytes (red algae) belonging to the order Corallinales [1]. With a distribution ranging from tropical latitudes to the high Arctic, they can be found in euphotic waters all over the world [2]. A characteristic trait of coralline algae is that they deposit calcium carbonate in the form of calcite [1, 3]. By depositing calcium carbonate, coralline algae create hard and sometimes three-dimensional structures, which may serve as habitats for other organisms. For this reason, they are considered important ecosystem engineers [2, 4-6].

As photoautotrophs [7], coralline algae rely on sunlight for survival. They are known to be efficient light harvesters, and have in clear oceanic waters been found at depths >250 m [8]. In terms of light harvesting, multicellular red algae have in general been shown to display highly similar absorbance spectra (i.e. optical signatures) [9]. Like most photoautotrophs, red algae partially rely on chlorophyll a (chl a) for light absorption [9]. Red algal chl a displays *in vivo* absorbance maxima at 437-439 nm (blue) and 678-681 nm (red), and a satellite band absorbance peak at ~630 nm (orange) [9, 10]. In addition to chl a,

phycobiliproteins contribute significantly to red algal light absorption. Phycobiliproteins are water-soluble pigments found in cyanobacteria, cryptomonads and red algae [11, 12], that mainly absorb light in the green region of the visible light spectrum (400-700 nm). Three major phycobiliprotein groups can be found in red algae: allophycocyanins, phycocyanins and phycoerythrins [13]. Of these, phycoerythrins are the most abundant [12]. Macrophytic red algae such as coralline algae are characterized by high contents of the phycoerythrin R-phycoerythrin (R-PE) [14]. R-PE strongly absorbs light in the blue-green region of the visible light spectrum, and displays absorbance maxima at 495-499 nm and 565-566 nm [15-17].

Currently, there exist several incentives for upscaling research on coralline algae. As ecosystem engineers [2, 4-6], their ecological importance is one of them. A conservation-related aspect, is that coralline algae as calcifiers may be adversely affected by ocean acidification [7, 18, 19]. Additionally, there is currently an interest in using coralline algae as biomarkers for assessing the impacts of discharges from oil platform drill cuttings on benthic habitats [20-22]. Regarding distribution, coralline algae are poorly mapped in certain regions of their range, including the Great Barrier Reef [23], the Arctic and the subarctic [6]. In a 2001 review paper by Foster [2], a need for long-term field studies of coralline algal habitats is also expressed. Because phycobiliproteins like R-PE are confined to a small range of organisms [11, 12], coralline algae can be considered spectrally conspicuous and therefore favorable targets for optical remote sensing. Underwater hyperspectral imaging represents a novel, optical remote sensing technique for marine environments [24, 25], which may be suitable for assessing coralline algae.

B. Underwater hyperspectral imaging

Over the past decades, hyperspectral imaging has become an established remote sensing technique for environmental mapping and monitoring [26-29]. The technique can be considered a form of spectroscopy capable of recording images as well as optical signatures. Hyperspectral imagers deployed on platforms such as airplanes and satellites have the ability to acquire high-resolution spectral data, which can be used for supervised classification of areas and objects of interest (OOIs). From aerial and space-borne platforms, hyperspectral image acquisition relies on the ambient light field generated by the sun. It can therefore be regarded as a passive imaging technique [30]. Dependency on ambient light has up until now restricted hyperspectral imaging to terrestrial and shallow-water environments. This is due to the optical properties of water, which quickly attenuate light as a function of depth [31]. Recently, an active version of the technique equipped with its own light source and a waterproof housing has however entered the scene of marine research: underwater hyperspectral imaging (UHI) [24]. Being independent of ambient light, UHI may be used for identifying, visualizing and mapping biogeochemical seafloor structures, which up until now have been out of reach from hyperspectral imagers.

The underwater hyperspectral imager is a push broom, camera-equipped spectrometer that receives light through a thin entrance slit. [32, 33]. During the process of capturing a hyperspectral image frame, light entering the instrument is diffracted into separate wavelengths, and projected onto the camera sensor as a contiguous spectrum. Each pixel row on the camera sensor parallel to the slit hence captures a picture of the slit at a particular wavelength. By tilting the frame 90° and instead collectively interpreting all the pixel rows as monochromatic levels of the same pixel row, the result is one hyperspectral pixel row corresponding to the light entrance slit, featuring detected intensities for all the utilized wavelengths [32]. In order to record image transects, the instrument is moved across the target area with the slit oriented perpendicularly to the direction of movement (push broom technique). As the instrument is moved, the camera continuously captures slit

frames at a set frame rate. An individual frame represents one cell (slit image) of the target area, and these frames are merged together to form continuous transects (photomosaic images) with a width dependent on slit width and the hyperspectral imager's altitude over the target area [32]. A transect can alternatively be interpreted as an image cube, where the x-, y- and z-axes respectively represent direction of movement, slit width and spectral levels [32]. Since each UHI pixel is assigned its own contiguous light spectrum, the spectral resolution and amount of information that can be obtained from an image transect is vastly increased [24]. As a result, UHI can detect subtle and otherwise unnoticeable spectral properties of a given OOI, and record object-specific optical fingerprints. Optical fingerprinting increases classification accuracy, and can be used for both qualitative and quantitative mapping during post-processing [24].

In addition to the spectral properties, spatial and radiometric properties also influence the resolution of underwater hyperspectral imagery [24]. The spatial resolution provided by UHI varies with altitude and sensor quality. Due to the rapid attenuation of light in the marine environment [31], underwater hyperspectral imagers are confined to scanning altitudes <10 m above the OOI. The focal plane of underwater hyperspectral imagers can be adjusted to distinguish between small-scale objects on a sub-meter scale, but even within the narrow underwater scanning range, the spatial resolution varies considerably with altitude. As a reference, a camera scanning distance of 2 m can potentially yield a spatial resolution close to 2 mm [24]. The exposure and color quality of UHI is partially determined by the imager's radiometric resolution (dynamic range in bits per pixel). Radiometric resolution varies between camera sensors, but is usually found within the interval of 8-16 bits per pixel [33]. A higher number of bits per pixel (e.g. 16) results in a broader dynamic range, and thus more accurate image depiction. However, high radiometric resolution also produces large data files, which may be hard to process and require extensive storage capacity. This tradeoff between quality and processability needs to be adjusted according to operational goals and computer processing capacity [24].

Being relatively compact instruments, underwater hyperspectral imagers are versatile in terms of deployment. Stationary platforms, such as tripods or rails with moving carts, mounted on the seafloor represent one of the most basic alternatives [24, 33, 34]. Mobile platforms equipped with dynamic positioning systems [35, 36] provide another layer of complexity by permitting larger areal coverage, and the possibility of temporal re-visitation through geolocation [24, 37]. Examples of mobile platforms used as UHI carriers include remotely operated vehicles (ROVs) and autonomous underwater vehicles (AUVs). Both represent state-of-the-art, instrument-carrying platforms for ocean exploration [37], with a survey range spanning from deep-sea trenches [38, 39] to ice-covered polar oceans [40-42]. The compatibility with underwater platforms capable of pushing exploration boundaries emphasizes the potential of UHI as a marine identification, mapping and monitoring tool, and suggests that the technology could play an important role for marine science in the future.

UHI technology has proven successful at visualizing and mapping a variety of OOIs and habitats. The versatility in application can partly be attributed to compact instrument design, providing flexibility in terms of deployment. From stationary platforms, underwater hyperspectral imagers may provide detailed imagery on small scales. In Hopavågen, Agdenes, Norway (April 2010), an underwater hyperspectral imager deployed on a rail-and-cart-based platform was for instance used to spectrally distinguish between various biogeochemical objects submerged for the occasion [24]. In Australia, tripod-based UHI operated by scuba divers has been used to assess the spectral characteristics of corals, stromatolites and sea grass *in situ* [33]. Although hyperspectral imagery from stationary platforms may be

highly informative, the true potential of UHI as a mapping tool first becomes apparent from mobile platforms such as ROVs. One of the benefits associated with ROV-based UHI mapping is its ability to cover larger areas that additionally may be beyond the reach of scuba diving and stationary platforms. ROV-based UHI was first attempted in 2012, and has since then been used for visualizing deep-water corals and archaeological sites in the Trondheimsfjord (Norway), coralline algal beds off Svalbard, and manganese nodules at 4,200 m depth in the Pacific Ocean [33, 37, 43]. With one successful pilot trial carried out [44], AUV-based UHI may provide yet another level of possibilities by permitting even larger areal coverage and increasing the degree of autonomy associated with hyperspectral image acquisition. Implementing UHI in AUV-based surveys could be considered the next step in underwater hyperspectral mapping, and will likely expand the technology's application potential in the future [33].

C. Optical properties of seawater

Due to the optical properties of seawater and its constituents, light is rapidly attenuated in the marine environment [31]. Two ways of looking at the optical properties are as apparent optical properties (AOPs), and inherent optical properties (IOPs). The AOPs are the optical properties of the medium in context with the geometrical structure of the ambient light field [45]. AOPs are measured with passive sensors, typically utilizing the light field generated by the sun [24]. In contrast, the IOPs are the optical properties of the medium alone, irrespective of the ambient light field [45]. IOPs are measured with active sensors equipped with a light source of known intensity and spectral composition (e.g. underwater hyperspectral imagers) [32]. Independence of ambient light makes IOPs especially relevant for dark environments [32], such as deep waters and the Arctic during the polar night. It also makes IOPs easier to interpret, because behavior of light is more readily quantifiable when the properties of the light source are known in detail [24].

D. Optical fingerprinting

During the process of optical fingerprinting, upwelling radiance and relative reflectance represent important physical parameters. Hyperspectral imagers measure upwelling radiance for each utilized wavelength of light [$L_u(\lambda)$, W m^{-2} nm^{-1} sr^{-1}]. When the spectral downwelling irradiance [$E_d(\lambda)$, W m^{-2} nm^{-1}] from the light source is known and all surfaces are assumed to behave as Lambertian reflectors, relative reflectance at a given wavelength [$R(\lambda)$, 0-1, where 1 represents 100% reflection] can be calculated with the following equation [24, 32].

$$R(\lambda) = \frac{\pi L_u(\lambda)}{E_d(\lambda)} \qquad \textbf{(1)}$$

Because $R(\lambda)$ is the ratio of $\pi L_u(\lambda)$ to $E_d(\lambda)$, it depends on light attenuation, and thus the IOPs of the water column, the light source spectrum and the light source intensity. In terms of IOPs, total volume attenuation (light beam attenuation) of a specific wavelength [$c(\lambda)$, m^{-1}] is the sum of light absorption [$a(\lambda)$] and scattering [$\beta(\lambda)$] in the medium [32]. Phytoplankton and water itself contribute to both absorption and scattering of photons, whereas colored dissolved organic matter (cDOM) and total suspended matter (TSM) contribute to absorption and scattering, respectively [32]. As the degree of attenuation increases exponentially with distance, the optical fingerprint of an OOI may vary substantially with both turbidity and scanning altitude [24]. One possible way of correcting for light source properties and the water column's impact on measurements and calculations, is applying a radiative transfer model on the acquired

spectral data [25, 46]. Another way is to deploy a reflectance plaque (reflectance standard) of known properties on the target area. Ideally, such a plaque should reflect light equally across the entire spectrum of visible light, so that attenuation of all wavelengths can be accounted for [24]. Knowing the upwelling radiance from a reference plaque [$L_{u\,ref}(\lambda)$] and assuming all surfaces behave as Lambertian reflectors, $R(\lambda)$ can be obtained with the equation

$$R(\lambda) = \frac{L_{u\,OOI}(\lambda)}{L_{u\,ref}(\lambda)}, \qquad \textbf{(2)}$$

where $L_{u\,OOI}(\lambda)$ represents the spectral upwelling radiance from the OOI [33, 34]. One potential downside to using Eq. 2 for reflectance estimation is that it fails to take into account the effects of light backscattered within the water column. These effects can be considered negligible when the distance between the sensor and the OOI is sufficiently short, but as the scanning distance increases, so does the impact of backscattered light on recorded measurements [47]. During post-processing of hyperspectral data, optical fingerprints can be used for qualitative as well as quantitative mapping. Hyperspectral mapping may be achieved by storing optical fingerprints of known organisms and OOIs as training sites in a spectral library, based on which supervised classification can be carried out [24, 48]. Classification can be based on both $L_u(\lambda)$ and $R(\lambda)$ spectra, but if the same training sites are to be used for multiple transects, $R(\lambda)$-based classification may be necessary to account for differences in IOPs and scanning altitude. During supervised classification, any pixel with an optical signature sufficiently close to the fingerprint of a library training site will be labelled as belonging to the respective OOI [49]. The spectra in the library hence allow for automated mapping of multiple OOIs in an efficient manner [34].

E. Experimental aims

The aim of this study was to assess the spectral characteristics of four coralline algal species, and to evaluate the potential of UHI as a coralline algal identification and mapping tool. Although multiple studies have previously featured spectral measurements of coralline algae [48, 50-53], species-specific comparisons of coralline algal optical signatures have to the authors' knowledge rarely been published. Previous studies have typically been carried out in shallow-water coral reef environments, and estimated the spectral reflectance of cm-dam-scale seafloor areas using either spectrometers *in situ* or aerial/space-borne imagery. In these studies, coralline algae have rightfully been characterized as one spectral group, owing to the purpose of the given study or limitations with respect to spatial resolution. For the purpose of the current study, species-specific spectral characteristics of coralline algae were however of interest due to the high spatial resolution of UHI, which permits even small (<1 cm) OOIs to be represented by multiple pixels. In the current study, spectrophotometry and high-performance liquid chromatography (HPLC) was used to verify the presence of important coralline algal pigments. The optical fingerprints of all four species were recorded in the form of $L_u(\lambda)$, using both a spectrometer and UHI. $L_u(\lambda)$ spectra from the two techniques were converted into $R(\lambda)$ to permit inter-instrumental as well as interspecific spectral comparisons. Multivariate statistical analyses were performed on various subsets of the $R(\lambda)$ data to identify the main wavelengths responsible for differences between species and instruments. Finally, using supervised classification, the coralline algal mapping potential of UHI was assessed both *in vivo* and *in situ*. Ultimately, the results of the study were used to answer whether 1) coralline algal $R(\lambda)$ could be related to pigment composition; 2) coralline algal species could be spectrally distinguished even though they are known to display similar optical properties [9]; 3) optical fingerprints recorded using different

instruments were comparable; and 4) UHI could be used to identify and map coralline algae.

2. MATERIALS AND METHODS

A. Laboratory-based spectral analyses

All laboratory-based spectral analyses were carried out at Trondheim Biological Station (TBS), at the Norwegian University of Science and Technology (NTNU). In the analyses, four species of coralline algae were investigated (Fig. 1): *Corallina officinalis* (Linnaeus, 1758), *Lithothamnion glaciale* (Kjellmann, 1883), *Phymatolithon lenormandii* (Areschoug, 1852) and *Phymatolithon tenue* (Rosenvinge, 1893). The former three were sampled in Hopavågen (63°35'N 9°32'E), Agdenes, Norway, in April 2016. All specimens from Hopavågen were sampled at depths between 1-5 m by scuba and freediving. *Phymatolithon tenue* was obtained from Trygghamna (78°14'N 13°50'E), Svalbard, Norway, in August 2016. Specimens of *P. tenue* were sampled at a depth of approximately 25 m by scuba diving.
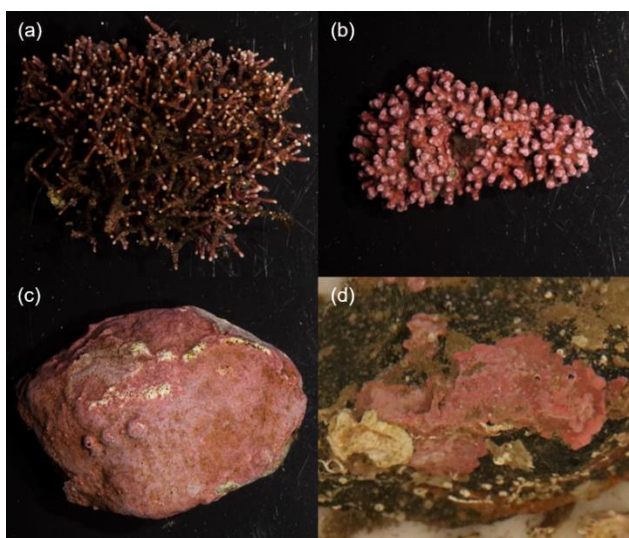

Fig. 1. The four coralline algal species analyzed spectrally: *Corallina officinalis* (a), *Lithothamnion glaciale* (b), *Phymatolithon lenormandii* (c) and *Phymatolithon tenue* (d).

Because the *P. tenue* specimens had to be transported by airplane from Svalbard to TBS, their health state was assessed upon arrival. The assessment was made using a pulse amplitude modulated (PAM) fluorometer (DIVING-PAM, Heinz Walz GmbH, Germany) according to the procedure described in Wägele and Johnsen (2001) [54]. Before the measurements, an autozero of the DIVING-PAM was performed. Measuring light frequency of chl a fluorescence was set to 0.6 kHz, which yielded non-actinic irradiance at 655 nm. Measuring light intensity was set to 10 (~0.15 µmol photons m^{-2} s^{-1}), whereas saturation flash intensity to close all photosystem (PS) II reaction centers was set to 12 (4,000 µmol photons m^{-2} s^{-1}). The operational quantum yield of chl a fluorescence from PS II ($\varphi'_{PS\ II}$) was measured under dim light conditions (~1 µmol photons m^{-2} s^{-1}). Measurements showed that *P. tenue*'s $\varphi'_{PS\ II}$ was 0.42 ± 0.07 (SD, n = 6), which proved the specimens were in good condition [21].

Prior to the analyses, the coralline algae were kept in a plastic crate flow-through system at TBS. The system was continuously provided sand-filtered seawater from a depth of 100 m, and held a temperature of 7-8°C. Dim sunlight provided illumination during daytime, and during midday, the system's underwater ambient light field was measured to

~1 µmol photons m^{-2} s^{-1}. Light intensity (irradiance from 400-700 nm) was measured using the DIVING-PAM irradiance sensor.

To verify the identity of characteristic coralline algal pigments, the pigment composition of *P. tenue* was assessed using both spectrophotometry (section 2.A.1.) and HPLC (section 2.A.2.). Ideally, the pigment composition of all four species should have been assessed, but due to limited laboratory access, only *P. tenue* pigments were characterized. The *P. tenue* pigments were considered representative also for the remaining three species, as red algae are known to display similar optical signatures [9]. The spectrophotometry was performed in seawater solvent, with the aim of identifying water-soluble phycobiliproteins *in vivo*. The remaining constituent pigments were investigated *in vitro*, using HPLC. Of the obtained coralline algae, six specimens of each species were chosen for $R(\lambda)$ analysis. Specimen-specific optical signatures [$L_u(\lambda)$ spectra] were recorded using both a spectrometer and UHI, and based on these signatures, mean $R(\lambda)$ spectra (n = 6) were calculated for each species, for both techniques.

1. In vivo *spectrophotometric pigment analysis*

A qualitative spectrophotometric analysis of water-soluble pigments in *P. tenue* was performed using a Unicam UV500 spectrophotometer (Thermo Fisher Scientific Inc., USA). Two algal specimens were crushed in separate mortars, containing approximately 100 mL of sand-filtered seawater each. The sand-filtered seawater served as both solvent and buffer. A 1-cm cuvette was used to characterize the pigments present in n = 3 syringe-filtered (0.2 µm, to remove particles), 3-mL phycobiliprotein extracts from each mortar (n = 6 extracts total). Absorbance in the cuvette samples was measured at 1-nm spectral resolution within the interval of 350-800 nm. The data were exported to Excel (Microsoft Corp., USA), where the absorbance spectrum from each cuvette sample was normalized by dividing all values by the respective sample's mean absorbance across all wavelengths. Normalized data were imported into the statistical software R, where a mean normalized absorbance spectrum (n = 6) with associated 95% confidence interval was calculated and visualized within the interval of 400-700 nm.

2. In vitro *HPLC pigment analysis*

Non-polar pigments in n = 6 *P. tenue* specimens were analyzed qualitatively *in vitro*, using a Hewlett Packard 1100 series HPLC system (Hewlett Packard Inc., USA), equipped with a diode array absorbance detector, according to Rodriguez et al. (2006) [55]. *Phymatolithon tenue* pigments were identified based on retention time and respective absorbance spectra, which were recorded at 1-nm spectral resolution within the interval of 350-700 nm. The data were exported to Excel, where each pigment-specific absorbance spectrum from each vial was normalized by dividing all values by the respective spectrum's mean absorbance across all wavelengths. Normalized data from the most dominant pigments were imported into the statistical software R, where mean normalized absorbance spectra (n = 6) with associated 95% confidence intervals were calculated and visualized within the interval of 400-700 nm.

3. In vivo *spectrometer analysis*

For the spectrometer analysis, a SpectroClip-JAZ-TR spectrometer (JAZ spectrometer, Ocean Optics Inc., USA) with a spectral resolution of approximately 0.3 nm, and a spectral range of 350-1,100 nm was used. All measurements were made using a QR400-7-VIS-BX reflection probe (Ocean Optics Inc., USA) connected to the spectrometer through an optical fiber bundle. The same bundle provided light to the tip of the reflection probe from a 20 W HL-2000-HP halogen light source (Ocean Optics Inc., USA). Spectrometer data (i.e. optical signatures) were

recorded using the software OceanView 1.5.2 (Ocean Optics Inc., USA). To optimize the signal-to-noise ratio, the integration time of each spectrometer scan was set to 3,000 µs, and boxcar width was set to 3. Boxcar smoothing averages adjacent pixels to increase signal-to-noise ratio at the expense of optical resolution [56]. A boxcar width of 3 implied that 7 pixels were averaged (3 to the left + 1 center + 3 to the right), which was considered a reasonable tradeoff between signal-to-noise ratio and optical resolution in the current study. In order to further smooth the spectral curves, scans to average per spectrometer measurement was set to 10. All spectrometer measurements were recorded perpendicularly to the OOI, at a distance of 2 cm. At this distance, the sampling area was ~0.79 cm² [57]. The measurements were recorded in a dark room to minimize the amounts of stray light interfering with the results. Remaining stray light was subtracted from the measurements using OceanView's "Dark spectrum" function.

As the spectrometer raw data were in the form of $L_u(\lambda)$, a spectrally neutral reference plaque was required for conversion into $R(\lambda)$ (Eq. 2). To carry out the conversion, a calibrated Spectralon (Labsphere Inc., USA) reflecting all wavelengths between 400-700 nm equally (~99%) was used in combination with a sanded (avoiding specular reflection), white polyethylene (PE) disk. The reason why the PE disk had to be included was that the Spectralon was unable to withstand immersion due to its porous material changing optical properties when saturated with water. Prior to the algal spectrometer analysis, the dry-state optical signatures of both reference plaques, as well as the in-water, immersed-state optical signature of the PE disk, were measured six times at a distance of 2 cm. Based on these measurements, a mean optical signature ($n = 6$) was assigned each reference plaque for each relevant set of conditions: $L_{u\ Spectralon\ dry}(\lambda)$, $L_{u\ PE\ dry}(\lambda)$ and $L_{u\ PE\ immersed}(\lambda)$. To account for the utilization of two reference plaques, Eq. 2 had to be modified before $R(\lambda)$ could be calculated. This was done by multiplying $R(\lambda)$ with the ratio of $L_{u\ PE\ dry}(\lambda)$ to $L_{u\ Spectralon\ dry}(\lambda)$, from now on referred to as PE:S(λ), as well as the known $R(\lambda)$ of the Spectralon (~0.99). Assuming that the measured optical signatures represented the actual optical signatures of the reference plaques, $R(\lambda)$ of the coralline algae could thus be calculated using the equation

$$R(\lambda) = \frac{L_{u\ OOI}(\lambda)}{L_{u\ PE\ immersed}(\lambda)} \times \frac{L_{u\ PE\ dry}(\lambda)}{L_{u\ Spectralon\ dry}(\lambda)} \times R_{Spectralon}(\lambda), \quad \textbf{(3)}$$

which further simplifies to

$$R(\lambda) = \frac{L_{u\ OOI}(\lambda) \times PE{:}S(\lambda) \times 0.99}{L_{u\ PE\ immersed}(\lambda)}. \quad \textbf{(4)}$$

Upon acquiring the reference data necessary for $R(\lambda)$ conversion, the coralline algae were analyzed with the spectrometer species by species. For each species, six specimens were examined under water, with the spectrometer at a distance of 2 cm. Together with the spectral data from the reference plaques, all algal optical signatures were exported from OceanView to Excel, where raw data were converted into $R(\lambda)$ using Eq. 4. Importing the $R(\lambda)$-converted data into the statistical software R, mean $R(\lambda)$ spectra ($n = 6$) with associated 95% confidence intervals were calculated for all algal species. Because the spectrometer analysis was carried out under highly controlled conditions, with minimal distance between the algae and the sensor, the JAZ spectrometer $R(\lambda)$ spectra were considered the control.

4. In vivo *UHI analysis*

The laboratory-based UHI analysis was performed using the hyperspectral imager UHI-1 (1st generation). UHI-1 was developed by Ecotone AS and is a solid-state hyperspectral imager fit into a 36 x 11 cm

cylindrical underwater housing, depth rated to 1,000 m. Copper wiring supplies power at 12 V, 0.4 A, while optical fiber bundles are responsible for signal transduction and electronic communication. Within UHI-1, a CCD-equipped (charge-coupled device) camera captures hyperspectral image frames through an 8-mm fore lens. For this study, UHI-1's lens aperture was set to f/2.8. The imager's spectral range spans from 380-800 nm, and with a 12-bit radiometric resolution, a dynamic range of 4,096 different intensities may be assigned each wavelength, detailed in Johnsen et al. (2016) [33].

In order to record hyperspectral image transects, UHI-1 was mounted on a motorized aluminum rig overlying a 2.0 x 1.0 x 1.5 m white plastic tank filled with sand-filtered seawater. The rig had been specifically designed for laboratory-based UHI applications by Ecotone AS, and was capable of moving the imager back and forth at different altitudes and speeds. In terms of lighting, the rig was equipped with two 250 W halogen lamps (220 V, one placed 13 cm away from the imager on each side) arranged in parallel to the light entrance slit of UHI-1. Once mounted, the imager was immersed to a scanning altitude of 40 cm. For each coralline algal species, the six specimens previously analyzed with the JAZ spectrometer were lined up directly beneath the imager's path of movement. In addition to the coralline algae, a sanded, white PE reference disk was placed at the bottom of the tank for $R(\lambda)$ conversion during post-processing. Upon setup completion, imaging adjustments and transect recordings were made using the software SpectralDAQ (Specim, Spectral Imaging Ltd., Finland). For the purpose of this survey, spectral resolution was set to 1 nm, while spatial resolution was set to 800 pixels per slit frame. The imager's frame rate was set to 44 Hz, whereas the exposure time was set to 21.7 ms. Transects were recorded by moving UHI-1 across the target area at a speed of approximately 6 cm s⁻¹. Recorded transects were stored as RAW files on an external hard drive.

Hyperspectral image transects were processed using the software ENVI 5.3.1 (Exelis Visual Information Solutions Inc., USA) in combination with Excel and the statistical software R. RAW files containing spectral information in the form of digital counts were converted into $L_u(\lambda)$, using the ENVI plug-in HYPERMAP developed by Ecotone AS. The $L_u(\lambda)$-converted transects had a spatial resolution of ~0.75 mm, and from the transects, a 32-pixel region of interest (ROI, ~0.18 cm²) was extracted from each specimen of each algal species. In addition, a 150-pixel ROI (~0.84 cm²) was extracted from the white PE reference disk. The mean optical signatures of all ROIs were imported into Excel, where specimen-specific algal $R(\lambda)$ was calculated using Eq. 4. The reason why $R(\lambda)$ was calculated external to ENVI was to make $R(\lambda)$ estimates from UHI as comparable as possible to estimates from the JAZ spectrometer. For the purpose of these $R(\lambda)$ calculations, $L_u(\lambda)$ from the 150-pixel PE reference ROI served as $L_{u\ PE\ immersed}(\lambda)$, whereas values for PE:S(λ) and $R_{Spectralon}(\lambda)$ were identical to the ones used in the JAZ spectrometer analysis. $R(\lambda)$-converted data were imported into the statistical software R, and based on intraspecific $R(\lambda)$ values, mean $R(\lambda)$ spectra ($n = 6$) with associated 95% confidence intervals were calculated for all algal species.

B. Field-based spectral analysis

Hyperspectral field data were collected during a polar night cruise to Svalbard in January 2016, with RV Helmer Hanssen (University of Tromsø). An underwater hyperspectral imager was deployed on NTNU's ROV Minerva [35, 58], and underwater hyperspectral image transects were recorded at 25-30 m depth in Trygghamna (78°14'N 13°50'E). Minerva was equipped with two 500 W high-intensity discharge (HID) lamps and a high-definition (HD) video camera for navigation and ground truthing. The observed benthic community was to a large degree dominated by coralline algae (no other macroalgal groups were observed), and based on video footage from Minerva, the

algae were classified as likely belonging to the species *P. tenue* (Fig. 2). Optical signatures of $n = 6$ algal specimens were extracted from the hyperspectral data, and based on these, a mean $R(\lambda)$ spectrum was calculated for the species.
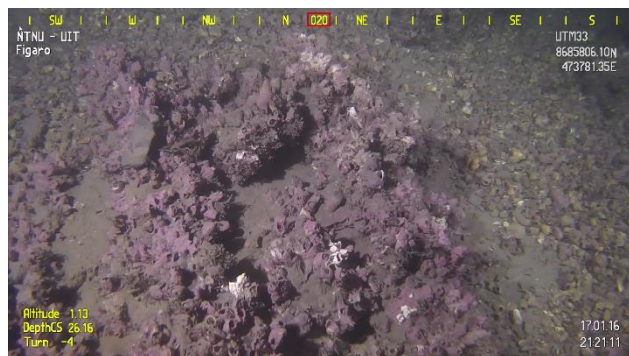

Fig. 2. ROV video footage from the January 2016 polar night cruise to Svalbard. The figure shows a frame grab from Trygghamna (78°14'N 13°50'E) containing the coralline algal species *Phymatolithon tenue*.

1. In situ *UHI analysis*

Field transects were recorded using the underwater hyperspectral imager UHI-2 (2nd generation). UHI-2 was developed by Ecotone AS, and is compared to UHI-1 a larger solid-state sensor, designed to fit into a 50 x 15.8 cm cylindrical underwater housing depth rated to 1,000 m. UHI-2 requires power at 12 V, 5 A, and like for UHI-1, copper wiring and optical fiber bundles are responsible for power supply and data transmission. Hyperspectral slit frames are captured through an 8-mm fore lens, and projected onto a scientific complementary metal-oxide semiconductor (sCMOS) camera sensor. For this study, UHI-2's lens aperture was set to f/2.8. The spectral range of UHI-2 is the same as for UHI-1 (380-800 nm), but the dynamic range is considerably larger: at 16-bit radiometric resolution, 65,536 different intensities may be assigned each utilized wavelength, further detailed in Johnsen et al. (2016) [33].

Prior to hyperspectral image acquisition, UHI-2 was mounted on the port side of Minerva, with the light entrance slit oriented in port-starboard direction. Two downward pointing, 250 W halogen lamps oriented 35 cm aft and fore of the imager provided UHI lighting. To permit conversion of hyperspectral field data into $R(\lambda)$ during post-processing, a spectrally neutral reference plaque was deployed on the seafloor. To accomplish this, a weighed down, black and white PE disk was brought to the survey site, using one of Minerva's manipulator arms. Once the survey site had been reached, the PE disk was dropped onto a flat area of interest. Using the SpectralDAQ software, the spectral resolution of UHI-2 was set to 2 nm, while spatial resolution was set to 800 pixels per slit frame. Frame rate and exposure time were set to 16 Hz and 25 ms, respectively. Minerva was manually maneuvered in straight transect lines across the area of interest, and hyperspectral imagery was recorded at an altitude of 1-2 m. All hyperspectral image transects were stored as RAW files on an external hard drive.

The obtained field data were processed in the same manner as data from the *in vivo* UHI analysis. In order to acquire algal $R(\lambda)$ data comparable to that from the JAZ spectrometer and UHI-1, a 3.75 x 1.40 m hyperspectral image transect recorded at ~25 m depth, at a steady altitude of 1.5 m was chosen for analysis. The chosen transect had a spatial resolution of ~1.75 mm, and contained both coralline algae and the PE reference disk. Using ENVI 5.3.1 and HYPERMAP, the RAW transect file was converted into $L_u(\lambda)$. 32-pixel ROIs (~0.98 cm² per ROI) were extracted from six algal specimens, and a 150-pixel ROI (~4.59 cm²) was extracted from the white area of the PE reference disk.

Mean optical signatures of all ROIs were exported to Excel, and converted into $R(\lambda)$ using Eq. 4 according to the procedure described for the *in vivo* UHI analysis. $R(\lambda)$-converted algal data were exported to the statistical software R, where a mean $R(\lambda)$ spectrum ($n = 6$) was calculated together with its 95% confidence interval.

C. Statistical comparison of reflectance spectra

In order to acquire a statistical overview of how different instruments and algal species related to each other spectrally, principal component analyses (PCAs) [59] were performed on three selections of $R(\lambda)$ data within the interval of 400-700 nm. The three data selections chosen for analysis were interspecific JAZ spectrometer $R(\lambda)$, inter-instrumental *Phymatolithon tenue* $R(\lambda)$ and all obtained $R(\lambda)$ data combined. With *in situ* data from UHI-2 being limiting, the PCAs had to be performed at approximately 2-nm spectral resolution. At this resolution, 155 wavelength variables were available. Because different instruments utilized marginally different wavelengths for recording light spectra, wavelengths from one instrument had to be matched with the closest corresponding wavelengths of the others. In the current study, the maximal wavelength difference between instruments was 0.53 nm. The PCAs were performed in the statistical software R, using the *prcomp* function from the built-in *stats* package. In order to reduce the impact of wavelengths where $R(\lambda)$ varied excessively between instruments (i.e. wavelengths were $R(\lambda)$ estimates were considered to be erroneous), data were standardized to mean = 0 (centered mean) and variance = 1 (scaled variance). The analyses were thus performed on correlation matrices. Results of the PCAs were visualized in biplots [60], using the *ggbiplot* function from the *ggbiplot* package available from GitHub (GitHub Inc., USA). In addition, the *facto_summarize* function from the *factoextra* package (GitHub) was used to quantify the relative contribution (%) of all wavelengths to variance explained by principal components (PCs) 1 and 2.

D. Supervised classification of coralline algae

Supervised classification of coralline algae in two hyperspectral image transects was carried out in ENVI. Both transects contained spectral data that had previously been used in the current study. The first transect chosen for classification had been used in the *in vivo* UHI-1 analysis, and contained the coralline algal species *C. officinalis*, *L. glaciale* and *P. lenormandii*. The second transect chosen for classification had been used in the *in situ* UHI-2 analysis, and contained the coralline algal species *P. tenue*. The spectral data in both transects were in the form of $L_u(\lambda)$. Although it is possible converting transects from $L_u(\lambda)$ to $R(\lambda)$ in ENVI through radiative transfer modelling, the classifications were based on $L_u(\lambda)$. The reason for this was that previous $R(\lambda)$ conversions had been performed external to ENVI (i.e. through Excel) and that an ENVI-based conversion could have produced species-specific $R(\lambda)$ spectra dissimilar from earlier estimates. By keeping the transects in $L_u(\lambda)$ form, classification could be carried out using the same coralline algal data that previously estimated $R(\lambda)$ spectra had been based on.

1. In vivo *supervised classification*

Supervised classification of a 2.00 x 0.60 m, *in vivo* UHI-1 transect containing *C. officinalis*, *L. glaciale* and *P. lenormandii* ($n = 6$ specimens per species) was carried out to assess UHI's ability to spectrally identify and distinguish between coralline algal species. A 32-pixel ROI had previously been extracted from each algal specimen in the transect to provide $L_u(\lambda)$ data for $R(\lambda)$ estimation. The same ROIs were chosen to serve as species-specific training sites for the classification. For each species, the mean optical signature of 192 ROI pixels (32 pixels per specimen, times $n = 6$ specimens) thus provided a class to be highlighted in the rest of transect. In addition to the species-specific classification, a

classification of coralline algae as a group was carried out for the same transect. For this classification, the mean optical signature of all 576 ROI pixels (192 pixels per species, times *n* = 3 species) served as the class to be highlighted. The statistical method chosen for the classifications was the spectral angle mapper (SAM), which is known to be suitable for classification of data of high spectral dimensionality [49]. In SAM, pixel spectra are treated as vectors in *n*-dimensional space, where *n* represents the number of wavelengths available. If the angle (radians) between a pixel spectrum and a training site spectrum falls within a user-defined maximum angle threshold, the pixel is classified as the corresponding OOI [61]. Thresholds were determined by visual photointerpretation, and following the algal classification procedure, both classifications were sieved to eliminate isolated pixels. Sieving in ENVI utilizes "blob grouping", which looks at the neighboring 4 or 8 pixels (pixel connectivity) to investigate whether a pixel is grouped with pixels belonging to the same class [62]. Pixel connectivity was in this case set to 8 pixels, whereas the minimum size of groups to keep was set to 16 pixels. Sieved classifications were exported from ENVI, and saved as TIFF files.

2. In situ *supervised classification*

To evaluate the ability of UHI to quantitatively assess coralline algal coverage *in situ*, supervised classification of *P. tenue* in a hyperspectral field transect was carried out in ENVI. The transect chosen was the 3.75 x 1.40 m, $L_u(\lambda)$-converted transect previously used in the *in situ* UHI-2 analysis of *P. tenue*. By using this transect, classification could be carried out using the same data that had been used to estimate *P. tenue*'s *in situ* $R(\lambda)$ spectrum. The six 32-pixel, *P. tenue* ROIs previously extracted thus served as a 192-pixel training site, providing an optical class/fingerprint to be identified in the remainder of the transect. A variety of statistical classification methods exist for hyperspectral imagery, and in this case, five different algorithms were chosen: SAM [61], minimum distance [49], binary encoding [63], spectral information divergence (SID) [64] and parallelepiped [49]. Classification thresholds were determined by visual photo-interpretation, and post-classification, all five classifications were sieved to eliminate isolated pixels. The sieving was carried out with the same settings as for the *in vivo* supervised classification. Percentage coralline algal coverage was extracted from each sieved classification, and the results were saved as TIFF files.

3. RESULTS

A. Laboratory-based spectral analyses

1. In vivo *spectrophotometric pigment analysis*

All *in vivo* spectrophotometric data revealed considerable *P. tenue* absorbance within the interval of ~450-580 nm. The normalized absorbance spectrum is shown in Fig. 3. Peaks in absorbance at 497 and 566 nm matched the *in vivo* absorbance maxima of the water-soluble phycobiliprotein R-PE [15-17].

2. In vitro *HPLC pigment analysis*

The *in vitro* HPLC analysis identified the presence of chl a, lutein, zeaxanthin, β-carotene, fucoxanthin, chlorophyll c and chlorophyll b-like pigments within the *P. tenue* extracts. Of these, chl a was by far the most abundant. Lutein was also present in considerable amounts, but the remaining pigments were only present in trace amounts. Normalized *in vitro* absorbance spectra of chl a and lutein are shown in Fig. 4. Chl a displayed strong absorbance peaks at 430 and 663 nm, and a shoulder at 413 nm. In addition, a notable satellite band absorbance peak was observed at 616 nm. For lutein, absorbance peaked at 448 and 476 nm, and a discernible shoulder was present at 426 nm.
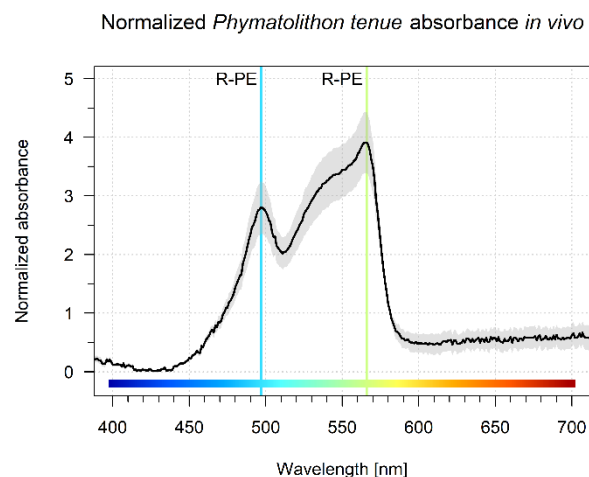

Fig. 3. Mean *in vivo* normalized absorbance spectrum (*n* = 6) of the coralline algal species *Phymatolithon tenue*. The gray shaded area represents the associated 95% confidence interval. Vertical lines represent *in vivo* absorbance maxima of the pigment R-phycoerythrin (R-PE) [15-17].
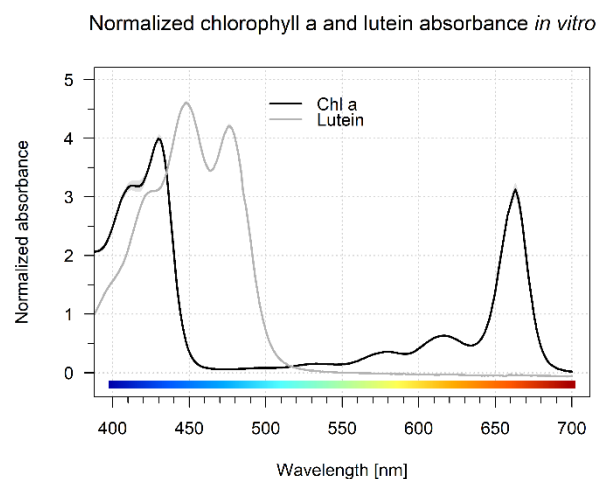

Fig. 4. Mean *in situ* normalized absorbance spectra (*n* = 6) of the *Phymatolithon tenue* pigments chlorophyll a (Chl a) and lutein. Gray shaded areas represent associated 95% confidence intervals.

3. In vivo *spectrometer analysis*

The *in vivo* spectrometer analysis produced coralline algal $R(\lambda)$ spectra with distinguished peaks and dips [Fig. 5(a)]. Except for slight amounts of noise present between ~400-440 nm, all calculated spectra appeared clean (high signal-to-noise ratio), with $R(\lambda)$ intensities ranging from 0.025-0.25. The main difference between species appeared to be $R(\lambda)$ intensity, as the spectral shapes of all algal spectra were highly similar. *Phymatolithon lenormandii* displayed the greatest overall $R(\lambda)$, followed by *P. tenue*, *L. glaciale* and *C. officinalis*, respectively. *Corallina officinalis* reflected considerably less light than the other three species within the interval of ~580-680 nm, and was thus the species standing out to the greatest extent. Regarding coralline algal light-harvesting capabilities, the four most pronounced $R(\lambda)$ dips were situated at approximately 438, 497, 566 and 679 nm. These dips

corresponded to the *in vivo* absorbance maxima of R-PE (497 and 566 nm) [15-17] and chl a (438 and 679 nm) [9, 10], and were prominent in the $R(\lambda)$ spectra of all four species. The weaker $R(\lambda)$ dip at ~629 nm corresponded to the *in vivo* satellite band absorbance peak of chl a [9].

4. In vivo *UHI analysis*

Between 500-700 nm, *in vivo* $R(\lambda)$ spectra from UHI-1 were comparable to those from the spectrometer analysis [Fig. 5(b)]. Coralline algal $R(\lambda)$ in the blue-wavelength region (<500 nm) did however differ considerably between the two instruments. For these wavelengths, UHI-1 $R(\lambda)$ values appeared greatly overestimated, peaking at ~0.58 between 415-420 nm. Disregarding the results from the blue-wavelength region, all $R(\lambda)$ intensities fell within the range of 0.1-0.25. As could be expected based on the results of the spectrometer analysis, all algal species produced spectra with highly similar shapes. Consequently, $R(\lambda)$ intensity once again appeared to be the main factor distinguishing the species. The greatest overall $R(\lambda)$ was displayed by the *Phymatolithon* spp., of which *P. tenue* was marginally more reflective. *Lithothamnion glaciale* and *C. officinalis* were the least reflective species, with *C. officinalis* displaying the lowest overall $R(\lambda)$. Relative to the other species, *C. officinalis* yielded particularly low $R(\lambda)$ between ~590-680 nm. In agreement with the *in vivo* spectrometer analysis results, this made *C. officinalis* the most spectrally conspicuous species. Marked $R(\lambda)$ dips situated at approximately 507, 575, 635 and 685 nm were observed in the spectra of all species. The observed dips corresponded to the absorbance of R-PE (507 and 575 nm) [15-17] and chl a (635 and 685 nm) [9, 10], but were red-shifted 5-10 nm compared to the pigments' expected *in vivo* absorbance peaks. As the obtained UHI-1 $R(\lambda)$ spectra invariably appeared red-shifted, the spectral shift was attributed to erroneous calibration of the instrument.

B. Field-based spectral analysis

1. In situ *UHI analysis*

Across all wavelengths, the UHI-2 *in situ* $R(\lambda)$ spectrum of *P. tenue* [Fig. 5(c)] was highly comparable to its equivalent spectrum from the *in vivo* spectrometer analysis. Besides from minor irregularities within the intervals of ~400-450 nm and ~540-550 nm, the spectrum appeared clean (high signal-to-noise ratio), with expected levels of $R(\lambda)$ intensity (0.1-0.3). The greatest dips in $R(\lambda)$ were observed at 437, 497, 566 and 678 nm, once again corresponding to the *in vivo* absorbance maxima of R-PE (497 and 566 nm) [15-17] and chl a (437 and 678 nm) [9, 10]. At ~629 nm, a weaker $R(\lambda)$ dip corresponding to chl a's *in vivo* satellite band absorbance peak [9] was also present.

C. Statistical comparison of reflectance spectra

The PCAs highlighted spectral differences between coralline algal species, and the results of the interspecific JAZ spectrometer PCA are shown in Fig. 6. In the corresponding biplot [Fig. 6(a)], all wavelength variables appeared to be strongly correlated, and PCs 1 and 2 respectively explained 95.9 and 2.9% of the variance. The groups of *L. glaciale*, *P. lenormandii* and *P. tenue* were clustered closely together, with significantly overlapping 95% confidence intervals. *Corallina officinalis* was the only group with an isolated 95% confidence interval, and accordingly, the only species with a potentially distinct optical signature. Figure 6(b) shows that variance explained by PC1 was close to equally distributed between wavelengths. Analysis of PC2 did however reveal that certain wavelengths had greater impacts than others [Fig. 6(c)], and especially the intervals of ~520-580 nm and ~600-660 nm had marked contributions to interspecific $R(\lambda)$ variance.
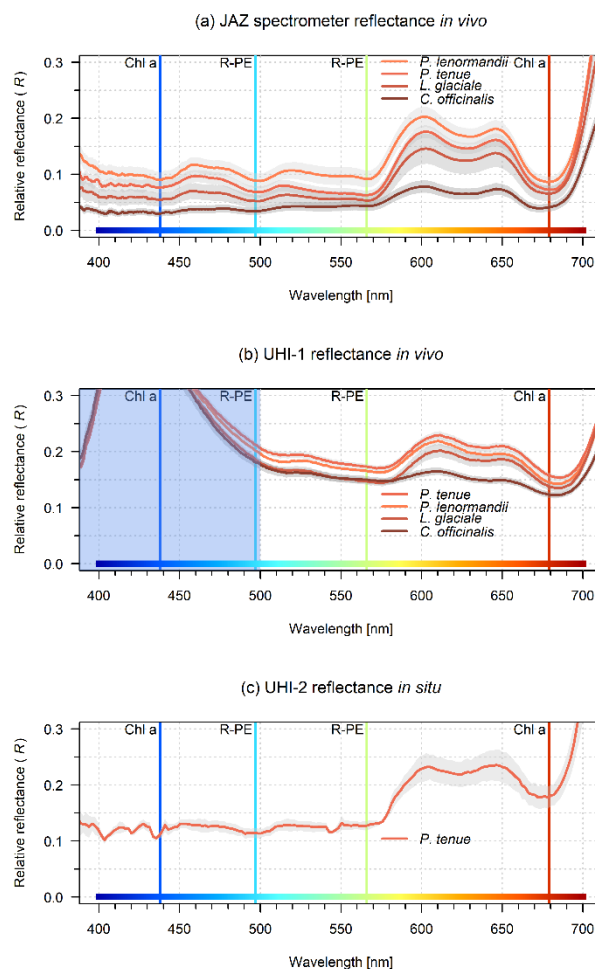

Fig. 5. Mean JAZ spectrometer (a), UHI-1 (b) and UHI-2 (c) reflectance [$R(\lambda)$] spectra (n = 6) of four coralline algal species: *Corallina officinalis*, *Lithothamnion glaciale*, *Phymatolithon lenormandii* and *Phymatolithon tenue*. JAZ spectrometer and UHI-1 $R(\lambda)$ spectra were obtained *in vivo*, and included all four species. UHI-2 $R(\lambda)$ spectra were obtained *in situ*, and only included *P. tenue*. Gray shaded areas represent the $R(\lambda)$ spectra's associated 95% confidence intervals. Vertical lines represent *in vivo* absorbance maxima of the pigments chlorophyll a (Chl a) [9, 10] and R-phycoerythrin (R-PE) [15-17]. The blue shaded area in panel (b) represents wavelengths where $R(\lambda)$ estimates from UHI-1 are considered to be overestimated (i.e. erroneous).

The PCAs also highlighted spectral differences between instruments, and results of the inter-instrumental *Phymatolithon tenue* PCA are shown in Fig. 7. In the associated biplot [Fig. 7(a)], it could be observed that blue-green wavelengths appeared correlated with PC1, and that far-red wavelengths appeared correlated with PC2. Regarding PC significance, PCs 1 and 2 explained 76.6 and 22.3% of the total $R(\lambda)$ variance, respectively. Of the three instrument groups, the groups of the JAZ spectrometer and UHI-2 were clustered most closely together. The UHI-1 group was completely isolated from the others, and differed mainly in the blue wavelengths. Figure 7(b) shows that wavelengths within the interval of ~460-580 nm were the main contributors to the variance explained by PC1. This corresponds to colors in the blue-green region of the spectrum. In addition, peaks in PC1 variance contribution were observed at approximately 620 and 670 nm. For PC2, wavelength contribution was greatest between ~590-700 nm, with peaks at ~595

nm, ~645 nm and in the far-red region of the spectrum [Fig. 7(c)]. Taking into consideration the distinct wavelength contributions to both PCs, the inter-instrumental $R(\lambda)$ variance appeared to be less uniformly distributed than the variance in the interspecific PCA (Fig. 6).
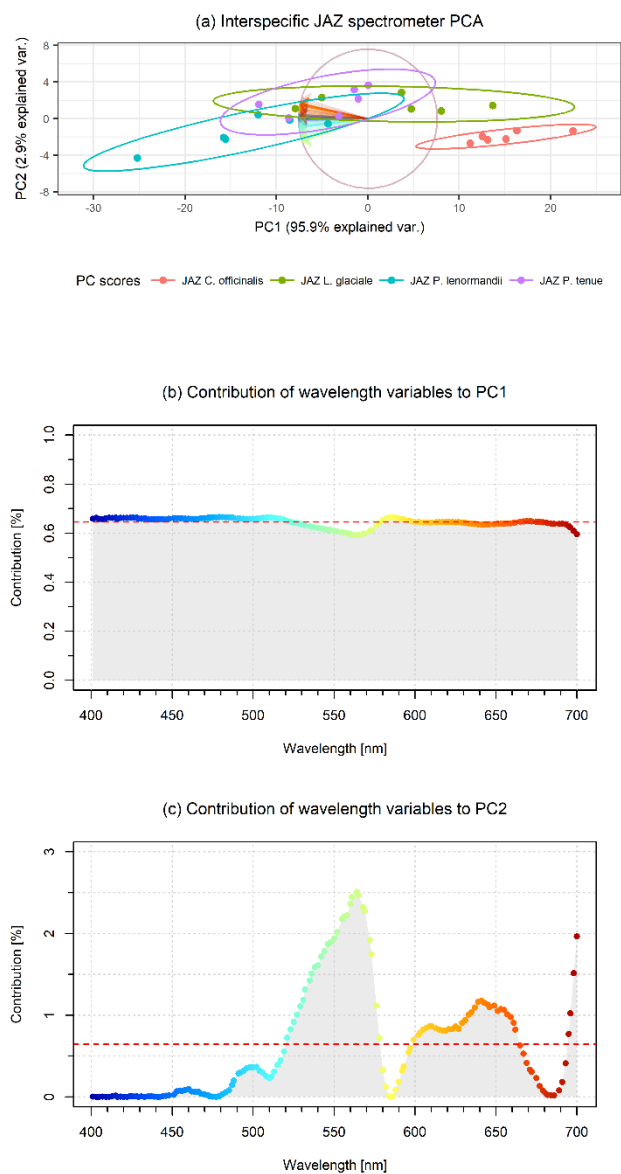

Fig. 6. Results of the principal component analysis (PCA) of interspecific JAZ spectrometer *in vivo* reflectance [$R(\lambda)$]. The analysis included $R(\lambda)$ data from four coralline algal species: *Corallina officinalis*, *Lithothamnion glaciale*, *Phymatolithon lenormandii* and *Phymatolithon tenue* (n = 6 specimens per species). Panel (a) shows a biplot of the PCA results. Points represent principal component (PC) scores [individual $R(\lambda)$ measurements], ellipses represent group-specific 95% confidence intervals, and colored arrows represent the different wavelength variables (n = 155). Arrows point in the direction of increasing $R(\lambda)$ intensity, and are colored according to their corresponding wavelengths. Panels (b) and (c) show relative contributions (%) of the wavelength variables to PCs 1 and 2. Red dashed lines represent expected wavelength contributions if contributions were uniform.
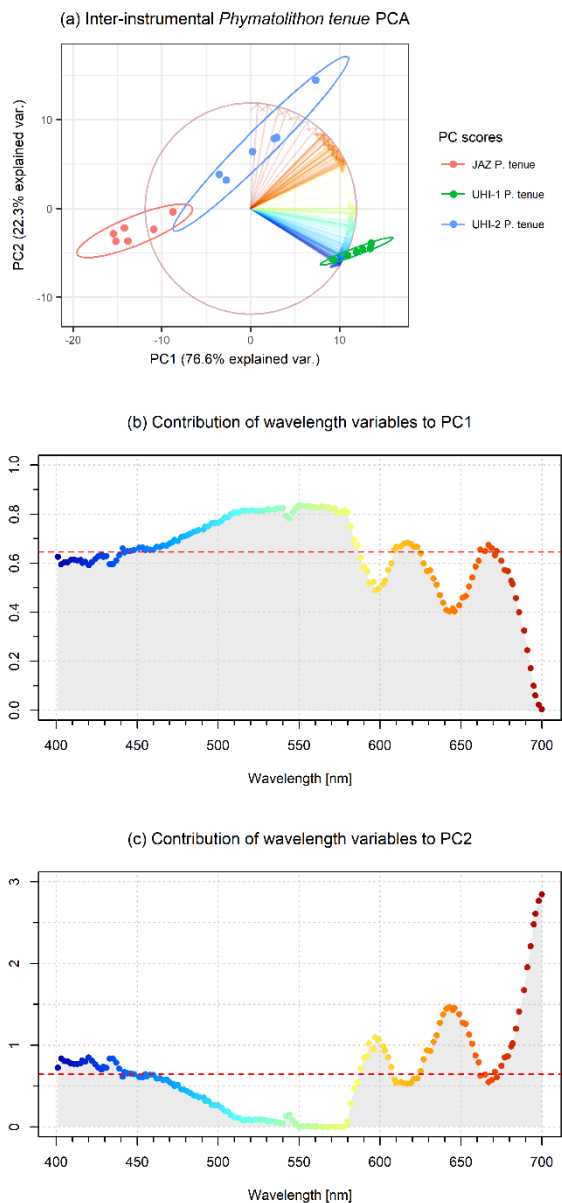

Fig. 7. Results of the principal component analysis (PCA) of inter-instrumental *Phymatolithon tenue* reflectance [$R(\lambda)$]. The analysis included $R(\lambda)$ data from three different instruments: the JAZ spectrometer *in vivo*, UHI-1 *in vivo* and UHI-2 *in situ* (n = 6 specimens per instrument). Panel (a) shows a biplot of the PCA results. Panels (b) and (c) show relative contributions (%) of the wavelength variables (n = 155) to PCs 1 and 2. A comprehensive description of the figure elements is presented in the Fig. 6 caption.

The final PCA encompassed $R(\lambda)$ data from all species and instruments combined, and the results are shown in Fig. 8. Overall, the results were highly comparable to those of the inter-instrumental *Phymatolithon tenue* PCA (Fig. 7). Based on the biplot [Fig. 8(a)], PCs 1 and 2 appeared correlated with blue-green and red wavelengths, respectively. PC1 explained 81.4% of the total variance, whereas PC2 explained 16.4%. Spectral measurements from the JAZ spectrometer and UHI-1 were assembled in separate clusters, and blue wavelengths appeared to be the main variables separating the two instruments. The

P. tenue group of UHI-2 had a slight overlap with the JAZ spectrometer cluster, but was separated from the measurements of UHI-1. Within the clusters of the JAZ spectrometer and UHI-1, the groups of *L. glaciale*, *P. lenormandii* and *P. tenue* were closely linked, with overlapping 95% confidence intervals. In accordance with the results of the interspecific JAZ spectrometer PCA [Fig. 6(a)], the only species with isolated or near-isolated groups was *C. officinalis*. As shown in Fig. 8(b), blue-green wavelengths within the interval of ~450-580 nm were the main contributors to the variance explained by PC1. Furthermore, peaks in variance contribution to PC1 were also observed at ~620 and ~670 nm. Figure 8(c) shows the different wavelengths' contribution to the variance explained by PC2. Here, contribution once again peaked at ~595 nm, ~645 nm and in the far-red region of the spectrum. The similarity between the results of the inter-instrumental *Phymatolithon tenue* PCA (Fig. 7) and the combined reflectance PCA suggests that the use of different instruments was a greater source of $R(\lambda)$ variance than coralline algal species.
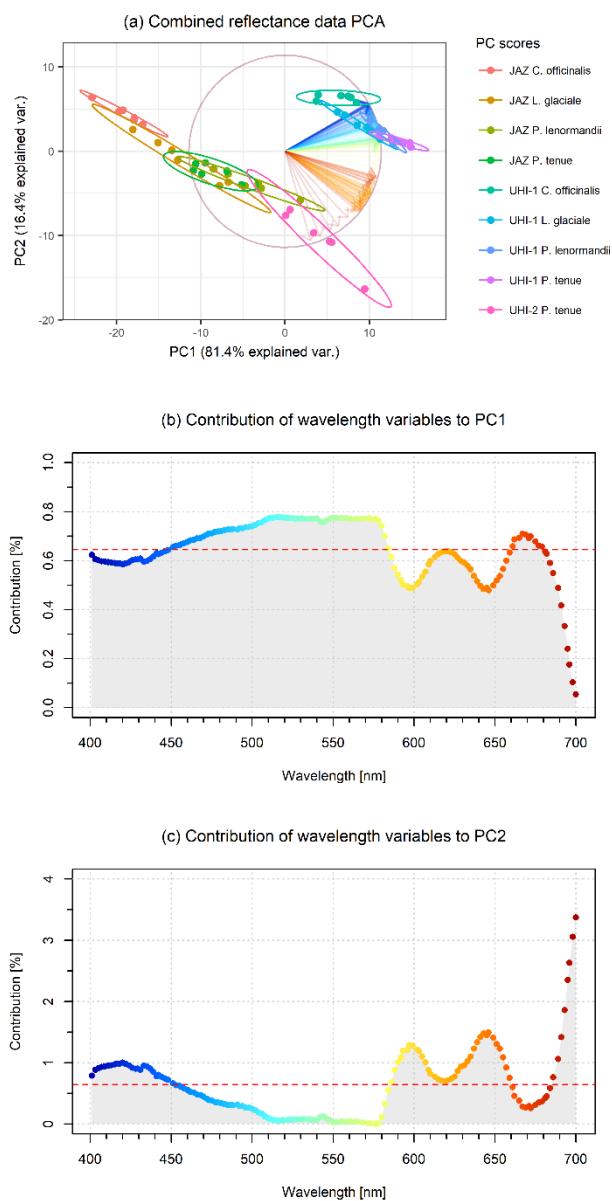

(a) Combined reflectance data PCA

(b) Contribution of wavelength variables to PC1

(c) Contribution of wavelength variables to PC2

Fig. 8. Results of the principal component analysis (PCA) of all reflectance [$R(\lambda)$] data combined. The analysis included $R(\lambda)$ data from four coralline algal species: *Corallina officinalis, Lithothamnion glaciale, Phymatolithon lenormandii* and *Phymatolithon tenue*. The $R(\lambda)$ data was acquired using three different instruments: the JAZ spectrometer *in vivo*, UHI-1 *in vivo* and UHI-2 *in situ* (*n* = 6 specimens per species, per instrument). Panel (a) shows a biplot of the PCA results. Panels (b) and (c) show relative contributions (%) of the wavelength variables (*n* = 155) to PCs 1 and 2. A comprehensive description of the figure elements is presented in the Fig. 6 caption.

An overview of percentage variance explained by PCs 1-3 in all PCAs is shown in Table 1. In all analyses, the first three PCs explained >99% of the total $R(\lambda)$ variance. Wavelength variables were most correlated in the interspecific JAZ spectrometer PCA, where PC1 explained close to 96% of the total variance. In contrast, the smallest degree of correlation was found in the inter-instrumental *Phymatolithon tenue* PCA, where <77% of the total variance was explained by PC1. Despite the high degree of correlation between variables in all PCAs, wavelength contribution to variance was, as shown in Figs. 6-8, not uniform. A noticeable trend [Figs. 6(c), 7(b-c) and 8(b-c)] was that the contribution appeared to coincide with the spectral properties of R-PE (Fig. 3) and chl a (Fig. 4). The impacts of specific pigments to $R(\lambda)$ variance are reviewed in discussion section 4.A. and C.

Table 1. Percentage coralline algal reflectance [$R(\lambda)$] variance explained by principal components (PCs) 1-3 in three PCAs.

PC#	Percentage $R(\lambda)$ variance explained by PCs 1-3		
	Interspecific JAZ spectrometer PCA	Inter-instrumental *Phymatolithon tenue* PCA	Combined reflectance data PCA
1	95.9	76.6	81.4
2	2.9	22.3	16.4
3	0.8	0.8	1.5
Sum	99.6	99.7	99.3

D. Supervised classification of coralline algae

1. In vivo supervised classification

Results of the *in vivo* supervised classification of coralline algae are displayed in Fig. 9. Figure 9(a) shows the training sites chosen to represent the spectral characteristics of *C. officinalis, L. glaciale, P. lenormandii* and coralline algae as a group. The results of the species-specific classification are shown in Fig. 9(b). *Corallina officinalis, L. glaciale*, and *P. lenormandii* were estimated to cover 0.41, 1.07 and 0.78% of the total transect area (2.26% combined), respectively. Although a trend in correct classification appeared to be present, the species-specific classification was unable to accurately distinguish between species. *Corallina officinalis* was partially misclassified as *L. glaciale* and *P. lenormandii* on two separate occasions. Furthermore, *L. glaciale* was frequently misclassified as *P. lenormandii*, and vice versa. *Lithothamnion glaciale* and *P. lenormandii* appeared to resemble each other more than *C. officinalis*, in that neither of the former two were misclassified as the latter to a considerable extent (four *L. glaciale* specimens were partially misclassified as *C. officinalis*, whereas *P. lenormandii* never was misclassified as *C. officinalis*). The degree to which classification suggested false negatives for regions corresponding to coralline algae, and false positives for regions not corresponding to coralline algae was minor, but present for all three species classes. Regarding the classification of coralline algae as a group [Fig. 9(c)], the overall pattern of classification was similar to that of Fig. 9(b). Compared

to the species-specific classification, group classification did however appear to produce a smaller number of false negatives, and a larger number of false positives. As a group, coralline algae were estimated to cover 3.95% of the total transect area, which was 1.69 percentage points higher than the combined estimate of the species-specific classifications.
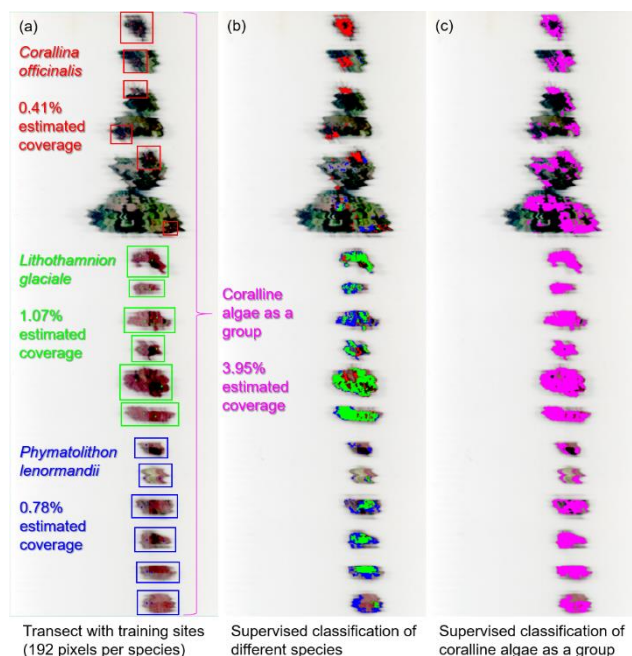
light field appeared to shift from blue to green, from left to right. This was caused by Minerva's HID lamps running simultaneously with the UHI halogen lamps. Illumination unevenness likely influenced classification at the outer margins of the transect, and thus, ultimately, the estimates of coralline algal areal coverage.

Transect with training sites
(192 pixels per species)

Supervised classification of
different species

Supervised classification of
coralline algae as a group

Fig. 9. Supervised classification of coralline algae *in vivo*, based on upwelling radiance $[L_u(\lambda)]$ from UHI-1. The 2.00 x 0.60 m hyperspectral image transect was recorded in a scanning tank. Species classifications were based on the mean $L_u(\lambda)$ signatures (n = 192 pixels per species) of *Corallina officinalis* (red), *Lithothamnion glaciale* (green) and *Phymatolithon lenormandii* (blue). The group classification was based on the mean $L_u(\lambda)$ signature (n = 576 pixels) of all three species combined (pink). Panel (a) shows the unclassified transect with training sites indicated by small dots (16 pixels per dot) highlighted according to species. Panel (b) shows the results of spectral angle mapper classification of different coralline algal species. Classified pixels are colored according to species. Panel (c) shows the results of spectral angle mapper classification of coralline algae as a group. Pixels classified as coralline algae are highlighted in pink. Estimated transect coverage (%) is shown for each class.

2. In situ *supervised classification*

Results of the *in situ* supervised classification displayed the potential of UHI as a coralline algal identification and mapping tool (Fig. 10). Estimates of coralline algal coverage in the $L_u(\lambda)$-converted UHI-2 transect [Fig. 10(a)] varied between classification algorithms, but always fell within the range of 5-10% of the total transect area. With an estimate of 10%, the binary encoding algorithm predicted the greatest coralline algal coverage [Fig. 10(d)]. SAM closely followed, with a coverage estimate of 8.79% [Fig. 10(b)]. The minimum distance [Fig. 10(c)], SID [Fig. 10(e)] and parallelepiped [Fig. 10(f)] algorithms predicted coralline algae to be less abundant, with coverage estimates of 6.50, 5.98 and 5.69% of the total transect area, respectively. Based on visual interpretation, the SAM and minimum distance algorithms appeared to provide the most accurate areal coverage estimates (i.e. the most favorable tradeoffs between coverage and misclassified pixels). However, none of the statistical classification methods were perfect. As can be observed in Fig. 10, the spectral characteristics of the transect

Transect with training sites
(192 pixels)

SAM
8.79% algal coverage

Minimum distance
6.50% algal coverage

Binary encoding
10.00% algal coverage

SID
5.98% algal coverage
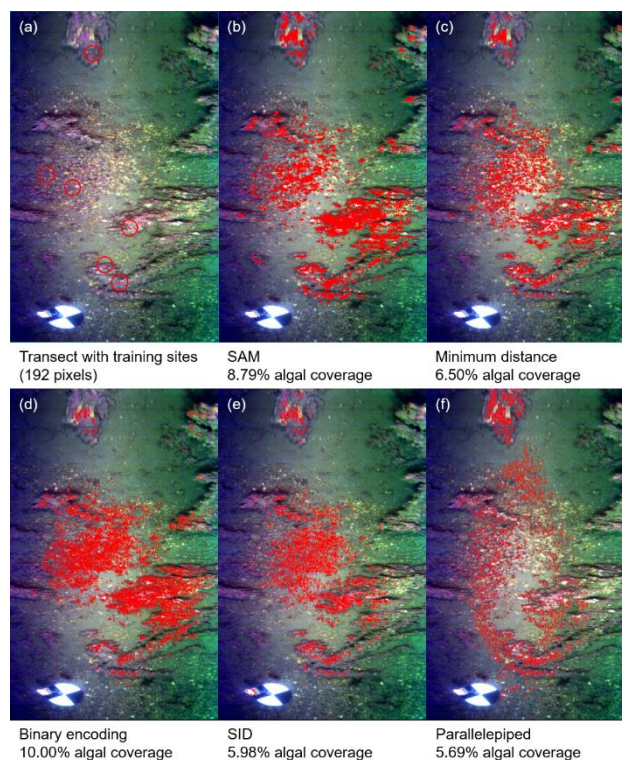
Parallelepiped
5.69% algal coverage

Fig. 10. Supervised classification of coralline algae *in situ*, based on upwelling radiance $[L_u(\lambda)]$ from UHI-2. Classification was based on the mean $L_u(\lambda)$ signature (n = 192 pixels) of *Phymatolithon tenue*. Panel (a) shows the unclassified transect with training sites (32 pixels within each circle) highlighted in red. Panels (b-f) show the classification results of four different algorithms: spectral angle mapper [SAM; (b)], minimum distance (c), binary encoding (d), spectral information divergence [SID; (e)] and parallelepiped (f). Pixels classified as *P. tenue* are highlighted in red, and the estimated coralline algal coverage (%) from each algorithm is shown below its respective panel.

4. DISCUSSION

A. Coralline algal pigments

Of the eight pigments discovered within the *P. tenue* extracts, two pigments appeared to be dominating coralline algal light absorbance: R-PE and chl a. Phycoerythrins are known to be the most abundant phycobiliproteins in many red algal species [12], and for macrophytic red algae, R-PE is thought to predominate [14]. For this reason, it came as no surprise that marked dips in $R(\lambda)$ (at approximately 497 and 566 nm) corresponding to the red algal *in vivo* absorbance maxima of R-PE [9, 10] could be observed in the spectra of all species (Fig. 5). The prevalence of R-PE was further verified by the *in vivo* absorbance spectrum of isolated, water-soluble *P. tenue* phycobiliproteins (Fig. 3), which closely resembled the absorbance spectrum of pure R-PE [15-17]. The lipophilic pigment fraction (fat soluble fraction, using organic solvents) of red algae is typically dominated by chl a and β-carotene [9]. Both pigments were detected in the *P. tenue* HPLC extracts, but chl a was considerably more abundant. Based on this information, dips

corresponding to the *in vivo* absorbance maxima of chl a were expected to be present in the coralline algal $R(\lambda)$ spectra. The *in vitro* absorbance spectrum of chl a (Fig. 4) displayed absorbance maxima at 430 and 663 nm, and a notable satellite band absorbance peak at 616 nm. Accounting for *in vitro* wavelength shifts [65], this amounts to *in vivo* absorbance maxima at approximately 438 and 677 nm, and an *in vivo* satellite band absorbance peak at approximately 630 nm. These wavelengths closely match the typical *in vivo* absorbance maxima of chl a in red algae [9, 10], and as expected, corresponding $R(\lambda)$ dips were prominent across all coralline algal species (Fig. 5). In addition to R-PE and chl a, lipophilic lutein was found to be present in *P. tenue* in considerable amounts. As the main dips in $R(\lambda)$ could be attributed to R-PE and chl a, the absorptive effects of lutein were less conspicuous. The HPLC revealed considerable *in vitro* lutein absorbance in the blue part of the spectrum, with peaks at 448 and 476 nm (Fig. 4). Considering that overall $R(\lambda)$ was low in this part of the spectrum [Fig. 5(a)], a reasonable hypothesis is thus that chl a and lutein harvested blue wavelengths in concert, but that the former was more abundant and overshadowed the specific dips attributed to lutein absorbance.

B. Overestimated *in vivo* UHI reflectance

Findings by Hochberg et al. (2003) [50] suggest that coralline algal $R(\lambda)$ of visible wavelengths typically ranges from 0-0.3. This range is exactly what was found for most wavelengths in the spectrometer and UHI spectra (Fig. 5), suggesting that the method used for $R(\lambda)$ conversion (Eq. 4) was adequate. There was however one notable exception: the blue-wavelength region of the UHI-1 $R(\lambda)$ spectra [Fig. 5(b)]. Blue-wavelength peak values were nearly twice as great as what could be expected based on the Hochberg et al. study [50], which indicates an error in measurement or the experimental setup. Overestimated $R(\lambda)$ of blue wavelengths had not been a problem in previous laboratory-based UHI surveys by Ecotone AS [66]. The light source used by Ecotone AS for similar rig and tank setups had however differed considerably from the one used in this study: whereas two 250 W halogen lamps provided illumination during the current *in vivo* UHI analysis, two 50 W halogen lamps had been used in equivalent surveys by Ecotone AS. It is thus possible that 500 W was an excessive amount of light in the confined space of the UHI tank. At a scanning distance of 40 cm, a significant proportion of this light was likely scattered randomly within the tank, and provided entry through the UHI slit, scattered light could have caused biased and overestimated UHI measurements by adding to the values of light reflected from the object directly beneath the imager. This claim is substantiated by $R(\lambda)$ intensity being greater for UHI-1 estimates than for JAZ spectrometer estimates (Fig. 5). Further indications supporting the hypothesis can be found in the fact that shorter wavelengths of light are scattered to a larger degree than longer wavelengths [67]. In addition, shorter wavelengths of visible light are typically absorbed by water to a far lesser extent than longer wavelengths [67]. This would imply that the proportion of blue-wavelength light scattered was larger than the proportion of green-to-red-wavelength light scattered. Following this reasoning, shorter-wavelength stray light entering the UHI slit would have the greatest impact on measurements, which is exactly what was observed. Excessive lighting may thus have been the reason for the overestimated UHI-1 $R(\lambda)$, and for future studies, light source intensity should be downscaled during laboratory-based UHI surveys.

C. Interspecific spectral differences

$R(\lambda)$ intensity appeared to be the main spectral characteristic separating coralline algal species. This could be observed within both the JAZ spectrometer [Fig. 5(a)] and the UHI-1 [Fig. 5(b)] $R(\lambda)$ spectra, where spectra of different species simply appeared to be intensity-shifted versions of the same spectrum. The interspecific JAZ

spectrometer PCA showed that wavelength variables were greatly correlated, and that different wavelengths were contributing approximately equally to the variance explained by PC1 [Fig. 6(b)]. In previous biological studies where spectral data have been analyzed using PCA, PC1 has traditionally been interpreted as brightness, i.e. differences in $R(\lambda)$ intensity between measurements [68-70]. Based on this interpretation, the interspecific PCA results thus showed that species differences in brightness were uniformly distributed between wavelengths, implying that spectral brightness differences between species were highly correlated. This corresponds well with the shape-wise, near-identical appearance of the spectra displayed in Fig. 5(a). Moreover, the fact that PC1 explained ~96% of the total variance in the interspecific PCA (Table 1) confirmed that $R(\lambda)$ intensity was the primary spectral characteristic distinguishing coralline algal species.

In terms of the reflective order of coralline algal species, similar patterns were observed within the JAZ spectrometer and the UHI-1 data. For both instruments, the two *Phymatolithon* spp. displayed the greatest overall $R(\lambda)$, followed by *L. glaciale* and *C. officinalis*, respectively. The only ambiguity was the reflective order of the former two. Whereas *P. lenormandii* was marginally more reflective when measured with the JAZ spectrometer [Fig. 5(a)], the opposite was true for UHI-1 [Fig. 5(b)]. Considering the highly controlled conditions under which the JAZ spectrometer measurements were made, it is likely the order displayed in Fig. 5(a) that is correct. The reason why UHI-1 produced a different order could have been that the assumed scanning distance was slightly off, which may have led to over- or underestimated measurements for one of the species. Nonetheless, differences in intensity order were marginal, and the overall relationship between species $R(\lambda)$ was very much consistent.

Looking past correlated differences in $R(\lambda)$ intensity between coralline algal species, the interspecific JAZ spectrometer PCA additionally revealed that certain wavelengths appeared to distinguish species to a greater extent than others. This was evident in the wavelength contribution plot for PC2, where especially wavelengths between ~520-580 nm (green-yellow) and, to some degree, wavelengths between ~600-660 nm (orange-red) dominated [Fig. 6(c)]. An interesting aspect of these findings is that the most dominant region of variance contribution was the green part of the spectrum. This region coincided well with the absorbance spectrum of R-PE both in terms of position and spectral shape (Fig. 3), which suggests that coralline algal R-PE content could serve as a means of separating species spectrally. Regarding the orange-red region of the spectrum, wavelength contribution to variance appeared to be inversely related to the *in vivo* red algal absorbance of chl a [9]. The position and shape of the spectral wavelength contribution in this region also corresponded well with the region *C. officinalis* $R(\lambda)$ appeared to differ the most from the equivalent $R(\lambda)$ of other species [Figs. 5(a-b)].

Upon establishing that some spectral differences appeared to exist between coralline algal species, an intriguing question became whether species could be spectrally distinguished with a sufficient degree of statistical certainty. Based on the biplot displayed in Fig. 6(a), the answer to this question is most likely no; at least with the available $R(\lambda)$ data. In the interspecific JAZ spectrometer PCA, the groups of *L. glaciale*, *P. lenormandii* and *P. tenue* were clustered closely together, and had largely overlapping 95% confidence intervals [Fig. 6(a)]. This suggests that the three species were closely related spectrally, which agrees well with the appearance of their associated $R(\lambda)$ spectra in Figs. 5(a-b). The only species that arguably could be spectrally distinguished from the rest, was *C. officinalis*. The *C. officinalis* group displayed a discrete optical signature in the Fig. 6(a) biplot, but was nonetheless positioned in the immediate vicinity of the *L. glaciale* group. Based on the current data set, none of the coralline algal species could thus be regarded as completely distinct spectrally. This does however not mean that statistically

significant differences do not exist. It is for instance important to acknowledge that $n = 6$ is a small sample size, and that photo acclimatization of the investigated specimens should have been elucidated with respect to pigment composition and bio-optical characteristics [71]. A considerable shortcoming of the current study regarding photo-acclimatizational effects, was that the coralline algae had been sampled from different depths and light regimes: *C. officinalis*, *L. glaciale* and *P. lenormandii* had been sampled from shallow waters (1-5 m) at temperate latitudes (63°N) during spring, whereas *P. tenue* had been sampled from deeper waters (~25 m) at Arctic latitudes (78°N) during the period of midnight sun. Ideally, all collected algae should have been acclimatized to the same light regime, so that intrinsic spectral properties truly would have been displayed. This, in combination with a larger sample size, could have produced different results. In the future, studies fulfilling these requirements should be carried out to further investigate if specific spectral characteristics, such as overall $R(\lambda)$ intensity or coralline algal content of R-PE, could serve as means of differentiating species statistically significantly.

D. Inter-instrumental spectral differences

Much like interspecific spectral variance, inter-instrumental spectral variance appeared to be dominated by differences in $R(\lambda)$ intensity. Even when disregarding the blue-wavelength region (400-500 nm) where UHI-1 $R(\lambda)$ was significantly overestimated, the spectra displayed in Fig. 5 show that estimated $R(\lambda)$ intensity close to invariably was greater for UHI measurements than for spectrometer measurements. Using the same PC interpretation [68-70] as for the interspecific PCAs, the inter-instrumental *Phymatolithon tenue* PCA (Fig. 7) confirmed that $R(\lambda)$ intensity truly was the main characteristic distinguishing measurements from different instruments, in that PC1 explained ~77% of the inter-instrumental $R(\lambda)$ variance (Table 1).

Although overall $R(\lambda)$ intensity could be considered the main spectral characteristic explaining inter-instrumental variance, wavelengths did not contribute equally to the differences between instruments. Results of the inter-instrumental *Phymatolithon tenue* PCA (Fig. 7) showed that wavelength contribution to the variance explained by PC1 [Fig. 7(b)] was not uniform like that of the interspecific PCA, but resembled an inverted depiction of the coralline algal $R(\lambda)$ spectra displayed in Fig. 5 ("pseudo-absorbance" of pigments). Blue-green (~460-580 nm) and, to some degree, bright-deep red (peaks at ~620 and ~670 nm) wavelengths contributed the most to variance explained by PC1. These wavelengths respectively correspond to regions of significant absorbance by R-PE and chl a (Figs. 3-4), which suggests a link between inter-instrumental variance and spectral regions of considerable light absorption [i.e. low $R(\lambda)$].

Based on the $R(\lambda)$ spectra displayed in Fig. 5, a marked difference between spectrometer and UHI results appeared to be the estimated lower values of coralline algal $R(\lambda)$. Whereas JAZ spectrometer data estimated coralline algal $R(\lambda)$ of certain wavelengths to be as low as ~0.025, equivalent UHI data never estimated $R(\lambda)$ to be lower than ~0.1. The reason for this could have been backscattered light adding to the true values of reflected light during UHI measurements. As the distance between sensor and OOI typically is greater for UHI measurements than for spectrometer measurements, there consequently is a greater water volume available for light to be backscattered during UHI surveys. Increased backscatter will in combination with the strong attenuation of light in water [31] result in a reduced signal-to-noise ratio, which potentially could affect measurements. Assuming that light backscatter by water and its constituents is constant regardless of the brightness of the object beneath the imager, the relative effects of backscatter will be greater when measuring darker objects. This is simply because backscattered light will make up a larger fraction of the total light entering the sensor

when the object beneath the imager absorbs light strongly. Although this example describes the phenomenon in relation to overall brightness, the same principle can be applied to hyperspectral measurements: assuming that wavelength-specific backscatter is constant regardless of the spectral properties of the OOI, the relative effects of backscatter on measured spectra will typically be greater for wavelengths strongly absorbed by the OOI. By the reasoning of this hypothesis, UHI measurements should produce $R(\lambda)$ spectra where $R(\lambda)$ is overestimated for all wavelengths due to the elevated backscatter associated with greater scanning distance. The degree of overestimation should however be greater for wavelengths strongly absorbed by the OOI, as backscatter will make up a larger fraction of the light measured at these wavelengths. Compared to an equivalent $R(\lambda)$ spectrum obtained using a spectrometer, a UHI $R(\lambda)$ spectrum can thus be expected to be upward-shifted, with a reduced lower-intensity range [especially in spectral regions where the given OOI displays its minimum $R(\lambda)$]. If the biased blue-wavelength region of UHI-1's $R(\lambda)$ spectra is disregarded, the postulated hypothesis fits exceptionally well with the results displayed in Fig. 5, and accounts for inter-instrumental $R(\lambda)$ differences in both overall intensity and lower intensity range. The hypothesis is further substantiated by the results of the inter-instrumental *Phymatolithon tenue* PCA, in which inter-instrumental variance was shown to be greatest for wavelengths where coralline algal pigments are known to absorb light strongly [Fig. 7(b)]. What can be concluded from these findings, is that a given OOI's apparent optical signature may be influenced by the distance between the object and the sensor. This does not necessarily mean that UHI-obtained spectra are inferior to spectrometer spectra obtained at short distances, but rather that spectra obtained from the two different techniques might not be directly comparable. For future, multi-instrumental studies of spectral characteristics in the marine environment, differences between instruments should be accounted for. Algorithms for backscatter compensation as a function of distance (e.g. the formulae presented by Maritorena et al. [47]) should be applied and further developed. For UHI, an accurate radiative transfer model synchronized with the position and altitude of the instrument platform may serve as a better means of obtaining true $R(\lambda)$ than reference disk-based conversion.

The fact that wavelength contribution to variance was less uniformly distributed in the inter-instrumental PCA [Fig. 7(b)] than in the interspecific PCA [Fig. 6(b)] suggests that instrument used was a greater source of variance than coralline algal species investigated. This claim is further supported by the biplots, where species-specific measurement clusters were shown to overlap to a large degree [Fig. 6(a)], whereas instrument-specific clusters hardly overlapped at all [Fig. 7(a)]. Results of the combined reflectance data PCA (Fig. 8) provided conclusive evidence that overall variance in the current data set was indeed dominated by the effects of instrument used. The wavelength contribution patterns of the combined reflectance PCA [Figs. 8(b-c)] were nearly identical to the wavelength contribution patterns of the inter-instrumental *Phymatolithon tenue* PCA [Figs. 7(b-c)], which implies a variance pattern dominated by inter-instrumental differences. This could also be observed in the biplot of the combined reflectance PCA, where interspecific measurements from the same instrument were clustered more closely together than inter-instrumental measurements of the same species [Fig. 8(a)]. Although overestimated $R(\lambda)$ of blue wavelengths and red-shifted $R(\lambda)$ spectra associated with the laboratory-based UHI-1 measurements undoubtedly reduced the accuracy of data obtained from UHI-1 and possibly led to overestimated inter-instrumental differences, the findings presented in this paragraph suggest that interspecific spectral differences may be interpreted in a biased manner if species are spectrally analyzed using different instruments and setups. If the focus is documenting the spectral relationship between species, measurements should therefore ideally

be recorded using the same instrument, under the same set of conditions.

E. Supervised classification and the potential of UHI-based mapping of coralline algae

Not surprisingly, the results of the *in vivo* supervised classification of different species fit well with the results of the interspecific PCA. In the biplot displayed in Fig. 6(a), all coralline algal species analyzed were shown to have closely related optical signatures (especially *L. glaciale* and *P. lenormandii*). Based on these findings, one could expect classification to have difficulty in distinguishing between coralline algal species. As shown in Fig. 9(b), this was exactly the case. Despite an evident pattern in correct classification, species were frequently misclassified. *Corallina officinalis* was misclassified to the smallest extent, but was nonetheless mistaken for both *L. glaciale* and *P. lenormandii*. *Lithothamnion glaciale* was regularly misclassified as *P. lenormandii*, and on four occasions as *C. officinalis*. *Phymatolithon lenormandii* was never misclassified as *C. officinalis*, but frequently as *L. glaciale*. Considering all this, and particularly that the largest degree of misclassification did in fact occur between *L. glaciale* and *P. lenormandii*, the biplot in Fig. 6(a) served as an excellent predictor for classification accuracy. It is possible that increasing the classification threshold for pixels to keep could have reduced the degree of misclassification, but doing so would also have resulted in an increased number of unclassified coralline algal pixels (i.e. false negatives). As false negatives were already present in the current species classification [Fig. 9(b)], the chosen threshold could therefore be considered a reasonable tradeoff between coverage and misclassification. In accordance with the results of the interspecific PCA, this study's supervised UHI classification thus suggests that coralline algal species cannot be spectrally distinguished with great accuracy.

Although the *in vivo* supervised UHI classification had difficulty in distinguishing between coralline algal species, it appeared capable of classifying coralline algae as a group. In the *in vivo* group classification [Fig. 9(c)], nearly all pixels corresponding to coralline algae were classified. By searching for one mean signature [Fig. 9(c)] instead of three species-specific signatures simultaneously [Fig. 9(b)], the estimate of total coralline algal coverage was increased from 2.26 to 3.95% of the total transect area. As the latter estimate contained fewer false negatives, group classification thus appeared superior to species classification in terms of coralline algal identification potential. The reduced number of false negatives did however appear to come at the price of an increased number of false positives. The number of falsely classified pixels in the group classification [Fig. 9(c)] was not overwhelming, but still appeared larger than the equivalent number from the species classification [Fig. 9(b)]. The reason for this was likely that averaging the optical signatures of multiple species yielded a more generic target for classification to identify. During group classification, a generic training site likely worked as a coarser sieve, including more coralline algal, as well as more non-coralline algal pixels. Once again, adjusting the classification threshold could have reduced the number of false positives, but as false negatives also were present in the results [Fig. 9(c)], the chosen threshold could be justified. Overall, the results of the *in vivo* supervised classification suggest that UHI has great potential as a coralline algal identification and mapping tool, which was further validated by the *in situ* supervised classification.

The *in situ* supervised UHI classification attempted to map *P. tenue* distribution in a 3.75 x 1.40 m transect. However, as *P. tenue* likely was the only coralline algal species present in the transect, the classification could also be considered as applying to coralline algae as a group (coralline algal pixels vs. non-coralline algal pixels). Based on visual interpretation of the results displayed in Fig. 10, supervised classification to a large degree appeared to be able to identify pixels

corresponding to coralline algae. The five different classification algorithms produced similar coverage and distribution estimates, which suggests that coralline algae could be identified and mapped also in their natural habitat. As the results of this study's UHI-based mapping of coralline algae can be considered promising, an interesting next step would be to carry out similar studies on larger scales and to monitor coralline algal habitats over time. Large-scale UHI surveys should also be conducted at sites dominated by corals, seagrass, macroalgae and stromatolites to further explore the utility of UHI as an environmental mapping tool.

Although the overall results of the *in situ* classification were favorable, certain issues were still present. As can be observed in Fig. 10, most of the classified pixels appeared to be concentrated in the transect interior. This could have been because coralline algae were only present in the interior of the transect, but as pixels containing coralline algae also appeared to be present along the margins of the transect, this was unlikely the case. A more feasible explanation was illumination unevenness, partially generated by the HID lamps of the ROV running simultaneously with the UHI halogen lamps. Towards the margins of the transect, light field conditions may have been biased to such an extent that pixels on the edges were not directly comparable to pixels in the interior. Assuming this, and considering that classification was based on *P. tenue* training sites situated far from the margins [Fig. 10(a)], it appears reasonable that coralline algal coverage was underestimated in marginal regions with low and biased illumination. Classification results were likely also influenced by minor differences in imaging altitude. As shown in Fig. 10, the area surveyed was not perfectly leveled. Unclassified pixels corresponding to coralline algae (i.e. false negatives) appeared to be especially abundant on objects protruding from the seafloor, which emphasizes the importance of maintaining a close to fixed distance between the sensor and the area of interest when hyperspectral imaging surveys are carried out in media where light is strongly attenuated, such as water [31]. A radiative transfer model capable of converting $L_u(\lambda)$ into $R(\lambda)$ based on real-time altitude data could possibly have accounted for this to some degree, but in highly heterogeneous seafloor habitats, classification accuracy will always be influenced by small-scale differences in altitude. The degree to which UHI classification is influenced by minor altitude differences resulting from seafloor heterogeneity should be investigated in the future. In the current study, choice of classification algorithm should be considered a final element of uncertainty. Although the four different classification algorithms yielded similar results, there were still differences between them. The SAM [Fig. 10(b)] and minimum distance [Fig. 10(c)] algorithms for instance appeared most efficient at accounting for light field differences (illumination unevenness), in that these algorithms were capable of classifying marginal pixels to a considerable extent without including an excessive number of false positives. For this reason, the coralline algal coverage estimates from the SAM and minimum distance algorithms were likely the most representative; a claim that agreed well with visual interpretation. As the purpose of the *in situ* supervised classification was to demonstrate the use of different algorithms rather than to quantify inter-algorithmic differences, the effects of algorithm choice will not be further discussed. It should however be noted that choice of algorithm has the potential to affect classification outcomes, and that this together with the effects of light field and altitude differences should be thoroughly considered for future UHI surveys.

As shown in this study, supervised classification represents a useful method for identifying and mapping OOIs with distinct optical signatures. A disadvantageous aspect of the method can however be the subjectivity associated with it. The accuracy of digital classifications has traditionally been determined by visual photointerpretation [72, 73], which was also the case in the current study. A considerable downside

to this approach is that the visual interpretation is assumed to be correct. Realistically, this may be far from the truth. In addition, an interpretation will depend on the human operator, which introduces a potential bias. During this study's supervised classifications, algorithm-specific threshold values were chosen solely based on subjective photointerpretation. The performance of the different classification algorithms was also assessed based on assumptions from visual interpretation. In more recent years, a variety of machine learning methods have been applied to improve the analysis of remote sensing imagery [73-75]. Machine learning methods have the potential to reduce the impact of selection biases and increase classification accuracy [75], and should therefore be considered for future classifications of underwater hyperspectral imagery.

Based on the results of the current study, there is little doubt that UHI may serve as a powerful tool for assessing coralline algal distribution. The spectral characteristics of coralline algae as a group appear conspicuous enough for them to be spectrally distinguished in their natural habitat, which permits mapping through optical fingerprinting and supervised classification. Although the current study suggests that high-accuracy, species-level mapping may not be achievable, information from group-level mapping may still be valuable. As an example, the distribution of coralline algae in the Arctic is poorly known, despite that coralline algae are believed to be the most dominant benthic calcifiers in high-latitude, euphotic waters [6]. Lacking knowledge of abundant species groups emphasizes the need for comprehensive mapping surveys, and provides an incentive for exploring the utility of state-of-the-art technologies such as UHI. In further support of future UHI-based mapping of coralline algae, there is currently a considerable effort aimed at increasing the autonomy and technological capabilities of underwater operations [76]. By deploying underwater hyperspectral imagers on AUVs, the survey range and data acquisition efficiency of UHI may for instance be significantly enhanced [33]. Moreover, the issues associated with this study's *in situ* classification can likely be avoided to a large degree by applying instrument platforms equipped with dynamic positioning systems and improved lighting, and refining the procedure for processing of underwater hyperspectral imagery. Taking all of this into account, the potential of UHI is evident, and coralline algae can be considered a suitable target for future underwater hyperspectral mapping surveys.

5. CONCLUSION

The four species of coralline algae investigated in the current study displayed highly similar spectral characteristics (optical fingerprints). Results of the study suggest that R-PE and chl a are the primary contributors to coralline algal light absorption. Both pigments were shown to be abundant in *P. tenue*, and dips corresponding to their expected absorbance maxima were prominent in the $R(\lambda)$ spectra of all species. The latter finding suggests that coralline algal $R(\lambda)$ is strongly linked to pigment composition.

Results of the multivariate statistical analyses suggest that different species of coralline algae are difficult to distinguish spectrally. It is however important to acknowledge that the current findings do not necessarily apply to all coralline algal species. The $R(\lambda)$ spectra of the investigated species were highly correlated, and mainly differed in overall brightness. Wavelengths corresponding to the region of R-PE light absorption were shown to contribute the most to interspecific spectral variance, but more comprehensive studies are needed to assess whether R-PE content can serve as a means of significantly differentiating coralline algal species.

Spectral data from UHI can be considered comparable to spectral data obtained using spectrometers under highly controlled laboratory conditions. Inter-instrumental spectral differences were however greater than spectral differences between coralline algal species.

Compared to a $R(\lambda)$ spectrum acquired up-close using a spectrometer, a $R(\lambda)$ spectrum acquired at greater distance using UHI can be expected to be overestimated in terms of intensity, with a reduced lower-intensity range. This is likely a consequence of backscattered light adding to the values of light reflected from the OOI; an effect that will have the greatest impact on $R(\lambda)$ estimates of wavelengths strongly absorbed by the OOI. For UHI spectral data to become more comparable to spectral data from spectrometers, software algorithms for backscatter compensation as a function of distance should be applied and further developed. An accurate radiative transfer model capable of converting $L_u(\lambda)$ into $R(\lambda)$ based on real-time position and altitude data from the instrument platform could possibly serve as a solution.

In vivo supervised classification was unable to accurately distinguish between coralline algal species in underwater hyperspectral imagery. Supervised classification of coralline algae as a group did however yield promising results both *in vivo* and *in situ*. This suggests that although coralline algal species may be spectrally difficult to differentiate, coralline algae as a group have a conspicuous optical signature that can be identified in UHI transects. Based on the surveys carried out in the current study, UHI can thus be considered a promising new technology, with great potential for mapping the distribution and abundance of coralline algae in their natural habitat.

In the future, research efforts aimed at improving our knowledge of coralline algae and the habitats they form should be increased. Coralline algae represent an ecologically important organism group [2, 4-6], that may be vulnerable to environmental change [7, 18, 19]. Currently, knowledge of coralline algal distribution and abundance is lacking [6, 23], and there is a need for more long-term studies [2, 20, 21]. The conspicuous spectral characteristics of coralline algae make them prime targets for optical remote sensing technologies such as UHI. In the future, UHI surveys aimed at mapping and monitoring coralline algal habitats should be carried out. Such surveys will not only enhance our understanding of ecosystems dominated by coralline algae, but also help establish UHI as a valuable tool for marine research. Although different species of coralline algae, and red algae in general [9], appear to display similar spectral characteristics, interspecific spectral differences should be further investigated. More comprehensive studies with higher species numbers, larger sample sizes and greater emphasis on coralline algal photo acclimatization could potentially reveal species-specific optical properties that passed by undetected in the current study. Such properties could permit optical mapping of coralline algae on a species level, which would be favorable for biodiversity studies. The current focus on increasing the autonomy and data acquisition efficiency of underwater operations [76] holds promise for future marine research, and suggests that large-scale coralline algal surveys could be conceivable in the near future.

References

1. P. C. Silva and H. W. Johansen, "A reappraisal of the order Corallinales (Rhodophyceae)," Brit. Phycol. J. **21**, 245-254 (1986).

2. M. S. Foster, "Rhodoliths: between rocks and soft places," J. Phycol. **37**, 659-667 (2001).

3. L. Le Gall and G. W. Saunders, "A nuclear phylogeny of the Florideophyceae (Rhodophyta) inferred from combined EF2, small subunit and large subunit ribosomal DNA: establishing the new red algal subclass Corallinophycidae," Mol. Phylogenet. Evol. **43**, 1118-1130 (2007).

4. C. G. Jones, J. H. Lawton, and M. Shachak, "Organisms as ecosystem engineers," Oikos **69**, 373-386 (1994).

5. S. Teichert, W. Woelkerling, A. Rüggeberg, M. Wisshak, D. Piepenburg, M. Meyerhöfer, A. Form, and A. Freiwald, "Arctic rhodolith beds and their environmental controls (Spitsbergen, Norway)," Facies **60**, 15-37 (2014).

6. H. I. Ø. Jørgensbye and J. Halfar, "Overview of coralline red algal crusts and rhodolith beds (Corallinales, Rhodophyta) and their possible ecological importance in Greenland," Polar Biol. **40**, 517-531 (2017).

7. L. Porzio, M. C. Buia, and J. M. Hall-Spencer, "Effects of ocean acidification on macroalgal communities," J. Exp. Mar. Biol. Ecol. **400**, 278-287 (2011).

8. M. M. Littler, D. S. Littler, S. M. Blair, and J. N. Norris, "Deepest known plant life discovered on an uncharted seamount," Science **227**, 57-60 (1985).

9. C. M. Smith and R. S. Alberte, "Characterization of in vivo absorption features of chlorophyte, phaeophyte and rhodophyte algal species," Mar. Biol. **118**, 511-521 (1994).

10. K. S. Beach, H. B. Borgeas, N. J. Nishimura, and C. M. Smith, "In vivo absorbance spectra and the ecophysiology of reef macroalgae," Coral Reefs **16**, 21-28 (1997).

11. K. S. Rowan, *Photosynthetic pigments of algae* (Cambridge University Press, Cambridge, UK, 1989), pp. 166-211.

12. A. N. Glazer, "Phycobiliproteins—a family of valuable, widely used fluorophores," J. Appl. Phycol. **6**, 105-112 (1994).

13. A. Glazer, "Light harvesting by phycobilisomes," Annu. Rev. Biophys. Biophys. Chem. **14**, 47-77 (1985).

14. T. A. Kursar and R. S. Alberte, "Photosynthetic unit organization in a red alga relationships between light-harvesting pigments and reaction centers," Plant Physiol. **72**, 409-414 (1983).

15. C. M. Hilditch, P. Balding, R. Jenkins, A. J. Smith, and L. J. Rogers, "R-phycoerythrin from the macroalga Corallina officinalis (Rhodophyceae) and application of a derived phycofluor probe for detecting sugar-binding sites on cell membranes," J. Appl. Phycol. **3**, 345-354 (1991).

16. A. V. Galland-Irmouli, L. Pons, M. Lucon, C. Villaume, N. T. Mrabet, J. L. Guéant, and J. Fleurence, "One-step purification of R-phycoerythrin from the red macroalga Palmaria palmata using preparative polyacrylamide gel electrophoresis," J. Chromatogr. B Biomed. Sci. Appl. **739**, 117-123 (2000).

17. R. Rossano, N. Ungaro, A. D'Ambrosio, G. M. Liuzzi, and P. Riccio, "Extracting and purifying R-phycoerythrin from Mediterranean red algae Corallina elongata Ellis & Solander," J. Biotechnol. **101**, 289-293 (2003).

18. I. B. Kuffner, A. J. Andersson, P. L. Jokiel, S. R. Ku'ulei, and F. T. Mackenzie, "Decreased abundance of crustose coralline algae due to ocean acidification," Nat. Geosci. **1**, 114 (2008).

19. W. A. Nelson, "Calcified macroalgae—critical to coastal ecosystems and vulnerable to change: a review," Mar. Freshwater Res. **60**, 787-801 (2009).

20. S. Johnsen, I. Nilssen, A. P. Brandao Pinto, and T. Torkelsen, "Monitoring of impact of drilling discharges to a calcareous algae habitat in the Peregrino oil field in Brazil," in *SPE International Conference on Health, Safety, and Environment*, (Society of Petroleum Engineers, 2014), 1-12.

21. I. Nilssen, F. dos Santos, R. Coutinho, N. Gomes, M. M. Cabral, I. Eide, M. A. Figueiredo, G. Johnsen, and S. Johnsen, "Assessing the potential impact of water-based drill cuttings on deep-water calcareous red algae using species specific impact categories and measured oceanographic and discharge data," Mar. Environ. Res. **112**, 68-77 (2015).

22. I. Nilssen, Ø. Ødegård, A. J. Sørensen, G. Johnsen, M. A. Moline, and J. Berge, "Integrated environmental mapping and monitoring, a methodological approach to optimise knowledge gathering and sampling strategy," Mar. Pollut. Bull. **96**, 374-383 (2015).

23. A. J. Dean, R. S. Steneck, D. Tager, and J. M. Pandolfi, "Distribution, abundance and diversity of crustose coralline algae on the Great Barrier Reef," Coral Reefs **34**, 581-594 (2015).

24. G. Johnsen, Z. Volent, H. Dierssen, R. Pettersen, M. Ardelan, F. Søreide, P. Fearns, M. Ludvigsen, and M. Moline, "Underwater hyperspectral imagery to create biogeochemical maps of seafloor properties," in *Subsea Optics and Imaging,* 1 ed., J. E. Watson and O. Zielinski, eds. (Woodhead Publishing Limited, Cambridge, UK, 2013), pp. 508-535.

25. J. Tegdan, S. Ekehaug, I. M. Hansen, L. M. S. Aas, K. J. Steen, R. Pettersen, F. Beuchel, and L. Camus, "Underwater hyperspectral imaging for environmental mapping and monitoring of seabed habitats," in *OCEANS 2015-Genova*, (IEEE, 2015), 1-6.

26. A. F. H. Goetz, "Three decades of hyperspectral remote sensing of the Earth: A personal view," Remote Sens. Environ. **113**, S5-S16 (2009).

27. P. R. C. Fearns, W. Klonowski, R. C. Babcock, P. England, and J. Phillips, "Shallow water substrate mapping using hyperspectral remote sensing," Cont. Shelf Res. **31**, 1249-1259 (2011).

28. M. P. Lesser and C. D. Mobley, "Bathymetry, water optical properties, and benthic classification of coral reefs using hyperspectral remote sensing imagery," Coral Reefs **26**, 819-829 (2007).

29. Y. Xie, Z. Sha, and M. Yu, "Remote sensing imagery in vegetation mapping: a review," J. Plant Ecol. **1**, 9-23 (2008).

30. T. Dickey, M. Lewis, and G. Chang, "Optical oceanography: recent advances and future directions using global remote sensing and in situ observations," Rev. Geophys. **44**, 1-39 (2006).

31. C. J. Funk, S. B. Bryant, and P. J. Heckman Jr, "Handbook of underwater imaging system design (TP-303)," (Ocean Technology Dept., Naval Undersea Center, San Diego, CA, USA, 1972).

32. G. Johnsen, Z. Volent, E. Sakshaug, F. Sigernes, and L. Pettersson, "Remote sensing in the Barents Sea," in *Ecosystem Barents Sea,* 2 ed., E. Sakshaug, G. H. Johnsen, and K. M. Kovacs, eds. (Tapir Academic Press, Trondheim, Norway, 2009), pp. 139-166.

33. G. Johnsen, M. Ludvigsen, A. Sørensen, and L. M. S. Aas, "The use of underwater hyperspectral imaging deployed on remotely operated vehicles-methods and applications," IFAC-PapersOnLine **49**, 476-481 (2016).

34. R. Pettersen, G. Johnsen, P. Bruheim, and T. Andreassen, "Development of hyperspectral imaging as a bio-optical taxonomic tool for pigmented marine organisms," Org. Divers. Evol. **14**, 237-246 (2014).

35. F. Dukan and M. Ludvigsen, "Dynamic positioning system for a small size ROV with experimental results," in *OCEANS, 2011 IEEE-Spain*, (IEEE, 2011), 1-10.

36. A. J. Sørensen, F. Dukan, M. Ludvigsen, D. A. Fernandez, and M. Candeloro, "Development of dynamic positioning and tracking system for the ROV Minerva," in *Further advances in unmanned marine vehicles,* 1 ed., G. N. Roberts and R. Sutton, eds. (The Institution of Engineering and Technology, London, UK, 2012), pp. 113-128.

37. M. Ludvigsen, G. Johnsen, A. J. Sørensen, P. A. Lågstad, and Ø. Ødegård, "Scientific operations combining ROV and AUV in the Trondheim Fjord," Mar. Technol. Soc. J. **48**, 59-71 (2014).

38. J. P. Barry and J. Hashimoto, "Revisiting the challenger deep using the ROV Kaiko," Mar. Technol. Soc. J. **43**, 77-78 (2009).

39. B. Fletcher, A. Bowen, D. R. Yoerger, and L. L. Whitcomb, "Journey to the challenger deep: 50 years later with the Nereus hybrid remotely operated vehicle," Mar. Technol. Soc. J. **43**, 65-76 (2009).

40. C. Kunz, C. Murphy, H. Singh, C. Pontbriand, R. A. Sohn, S. Singh, T. Sato, C. Roman, K. i. Nakamura, and M. Jakuba, "Toward extraplanetary

under-ice exploration: Robotic steps in the Arctic," J. Field Robot. **26**, 411-429 (2009).

41. C. Kaminski, T. Crees, J. Ferguson, A. Forrest, J. Williams, D. Hopkin, and G. Heard, "12 days under ice–an historic AUV deployment in the Canadian High Arctic," in *Autonomous Underwater Vehicles (AUV), 2010 IEEE/OES*, (IEEE, 2010), 1-11.

42. P. Norgren and R. Skjetne, "Using Autonomous Underwater Vehicles as Sensor Platforms for Ice-Monitoring," Model. Ident. Control **35**, 263-277 (2014).

43. I. N. Dumke, S. M., A. Purser, Y. Marcon, M. Ludvigsen, S. L. Ellefmo, G. Johnsen, and F. Søreide, "First hyperspectral imaging survey of the deep seafloor: high-resolution mapping of manganese nodules," Remote Sens. Environ. (under review) (2017).

44. Ø. Sture, M. Ludvigsen, F. Søreide, and L. M. Sandvik Aas, "Autonomous underwater vehicles as a platform for underwater hyperspectral imaging," in *OCEANS 2017 MTS/IEEE, Aberdeen, UK,* (IEEE, 2017), pp. 1-8.

45. R. W. Preisendorfer, "Hydrologic Optics. Volume 1. Introduction," (US Dept. of Commerce, National Oceanic and Atmospheric Administration, Environmental Research Laboratories, Pacific Marine Environmental Laboratory, Honolulu, HI, USA, 1976).

46. C. D. Mobley and D. Stramski, "Effects of microbial particles on oceanic optics: Methodology for radiative transfer modeling and example simulations," Limnol. Oceanogr. **42**, 550-560 (1997).

47. S. Maritorena, A. Morel, and B. Gentili, "Diffuse reflectance of oceanic shallow waters: influence of water depth and bottom albedo," Limnol. Oceanogr. **39**, 1689-1703 (1994).

48. T. Kutser, I. Miller, and D. L. B. Jupp, "Mapping coral reef benthic substrates using hyperspectral space-borne images and spectral libraries," Estuar. Coast. Shelf Sci. **70**, 449-460 (2006).

49. J. A. Richards, *Remote sensing digital image analysis*, 5 ed. (Springer-Verlag Berlin Heidelberg, Berlin, Germany, 1999), pp. 166-211.

50. E. J. Hochberg, M. J. Atkinson, and S. Andréfouët, "Spectral reflectance of coral reef bottom-types worldwide and implications for coral reef remote sensing," Remote Sens. Environ. **85**, 159-173 (2003).

51. S. Andréfouët, C. Payri, E. J. Hochberg, C. Hu, M. J. Atkinson, and F. E. Muller-Karger, "Use of in situ and airborne reflectance for scaling-up spectral discrimination of coral reef macroalgae from species to communities," Mar. Ecol. Prog. Ser. **283**, 161-177 (2004).

52. I. A. Leiper, S. R. Phinn, and A. G. Dekker, "Spectral reflectance of coral reef benthos and substrate assemblages on Heron Reef, Australia," Int. J. Remote Sens. **33**, 3946-3965 (2012).

53. I. A. Leiper, S. R. Phinn, C. M. Roelfsema, K. E. Joyce, and A. G. Dekker, "Mapping coral reef benthos, substrates, and bathymetry, using compact airborne spectrographic imager (CASI) data," Remote Sens. **6**, 6423-6445 (2014).

54. H. Wägele and G. Johnsen, "Observations on the histology and photosynthetic performance of "solar-powered" opisthobranchs (Mollusca, Gastropoda, Opisthobranchia) containing symbiotic chloroplasts or zooxanthellae," Org. Divers. Evol. **1**, 193-210 (2001).

55. F. Rodriguez, M. Chauton, G. Johnsen, K. Andresen, L. Olsen, and M. Zapata, "Photoacclimation in phytoplankton: implications for biomass estimates, pigment functionality and chemotaxonomy," Mar. Biol. **148**, 963-971 (2006).

56. Ocean Optics Inc., "Glossary" (2017), retrieved August 14, 2017, https://oceanoptics.com/glossary/.

57. Ocean Optics Inc., "Sampling Accessories for Reflection" (2017), retrieved August 14, 2017, https://oceanoptics.com/sampling-accessories-for-reflection/.

58. M. Ludvigsen, "An ROV toolbox for optical and acoustical seabed investigations," PhD thesis (Norwegian University of Science and Technology (NTNU), 2010).

59. H. Hotelling, "Analysis of a complex of statistical variables into principal components," J. Educ. Psychol. **24**, 417-441 (1933).

60. K. R. Gabriel, "The biplot graphic display of matrices with application to principal component analysis," Biometrika **58**, 453-467 (1971).

61. F. A. Kruse, A. B. Lefkoff, J. W. Boardman, K. B. Heidebrecht, A. T. Shapiro, P. J. Barloon, and A. F. H. Goetz, "The spectral image processing system (SIPS)—interactive visualization and analysis of imaging spectrometer data," Remote Sens. Environ. **44**, 145-163 (1993).

62. Harris Geospatial Solutions, "Sieve classes" (2017), retrieved August 14, 2017, https://www.harrisgeospatial.com/docs/SievingClasses.html.

63. A. S. Mazer, M. Martin, M. Lee, and J. E. Solomon, "Image processing software for imaging spectrometry data analysis," Remote Sens. Environ. **24**, 201-210 (1987).

64. Y. Du, C.-I. Chang, H. Ren, C.-C. Chang, J. O. Jensen, and F. M. D'Amico, "New hyperspectral discrimination measure for spectral characterization," Opt. Eng. **43**, 1777-1786 (2004).

65. G. Johnsen, N. B. Nelson, R. V. M. Jovine, and B. B. Prezelin, "Chromoprotein-and pigment-dependent modeling of spectral light absorption in two dinoflagellates, Prorocentrum minimum and Heterocapsa pygmaea," Mar. Ecol. Prog. Ser., 245-258 (1994).

66. I. M. Hansen, Ecotone AS, Havnegata 9, NO-7010 Trondheim, Norway (personal communication, 2017).

67. A. Morel, "Optical properties of pure water and pure sea water," in *Optical Aspects of Oceanography,* 1 ed., N. G. Jerlov and E. S. Nielsen, eds. (Academic Press, Madison, WI, USA, 1974), pp. 1-24.

68. J. A. Endler and M. Thery, "Interacting effects of lek placement, display behavior, ambient light, and color patterns in three neotropical forest-dwelling birds," Am. Nat. **148**, 421-452 (1996).

69. S. Hunt, A. T. D. Bennett, I. C. Cuthill, and R. Griffiths, "Blue tits are ultraviolet tits," Proc. R. Soc. Lond. B Biol. Sci. **265**, 451-455 (1998).

70. C. P. Grill and V. N. Rush, "Analysing spectral data: comparison and application of two techniques," Biol. J. Linn. Soc. **69**, 121-138 (2000).

71. G. Johnsen, A. Bricaud, N. Nelson, B. B. Prézelin, and R. R. Bidigare, "In vivo bio-optical properties of phytoplankton pigments," in *Phytoplankton pigments: Characterization, chemotaxonomy and applications in oceanography,* 1 ed., S. Roy, C. A. Llewellyn, E. S. Egeland, and G. Johnsen, eds. (Cambridge University Press, Cambridge, UK, 2011), pp. 497-537.

72. R. G. Congalton, "A review of assessing the accuracy of classifications of remotely sensed data," Remote Sens. Environ. **37**, 35-46 (1991).

73. D. Tuia, M. Volpi, L. Copa, M. Kanevski, and J. Munoz-Mari, "A survey of active learning algorithms for supervised remote sensing image classification," IEEE J. Sel. Topics Signal Process. **5**, 606-617 (2011).

74. M. M. Crawford, D. Tuia, and H. L. Yang, "Active learning: Any value for classification of remotely sensed data?," Proc. IEEE **101**, 593-608 (2013).

75. C. Persello and L. Bruzzone, "Active and semisupervised learning for the classification of remote sensing images," IEEE Trans. Geosci. Remote Sens. **52**, 6937-6956 (2014).

76. M. Ludvigsen and A. J. Sørensen, "Towards integrated autonomous underwater operations for ocean mapping and monitoring," Annu. Rev. Control **42**, 145-157 (2016).